Univerzita Karlova v Praze

Přírodovědecká fakulta

Studijní program: Vývojová biologie (P1520)

Studijní obor: Vývojová biologie (1501V000)

Oleksandr Chernyavskiy

Zdokonalené metody pro snímání obrazových dat a analýzu tkání a buněk

pomocí konfokální a multifotonové mikroskopie

Improved Methods of Image Acquisition and Analysis of Tissues and Cells

by Confocal and Multi-Photon Microscopy

Disertační práce

Školitel: RNDr. Lucie Kubínová CSc

Praha, 2015

Prohlášení:

Prohlašuji, že jsem závěrečnou práci zpracoval samostatně a že jsem uvedl všechny použité informační zdroje a literaturu. Tato práce ani její podstatná část nebyla předložena k získání jiného nebo stejného akademického titulu.

V Praze, 22.02.2015

Podpis

Acknowledgments

Table of Contents

Abbreviations and acronyms

1PE – one-photon excitation

2P-CM, 2PCM – two-photon confocal microscopy

2PE – two-photon excitation

3D – three-dimensional

BCP – bromcresol purple

BP400/15 (BP430/15, BP525/50, BP610/75) – band-pass optical filter with the center of the transmittance window of 400 (430, 525, 610) nm and the full width at half maximum of the transmission curve 15 (15, 50, 75) nm respectively

CCD – a charge coupled device, a light-sensitive integrated circuit, used as a sensor used in digital cameras and video cameras

CLSM – confocal laser scanning microscopy

ConA-AF or ConA – lectin (or sugar binding protein) Concanavalin A conjugated with Alexa Fluor 488

DD – descanned detection or descanned detector

ECM – extracellular matrix

FCS – fluorescence correlation spectroscopy

FLIM – fluorescence lifetime imaging

FLIP – fluorescence loss in photobleaching

FRAP – fluorescence recovery after photobleaching

FRET – Förster (fluorescence) resonance energy transfer

FITC – Fluorescein isothiocyanate

GaAsP – gallium arsenide phosphide photodiode

GFP – green fluorescent protein

H&E or HE – hematoxylin and eosin staining

HeNe – helium neon (laser)

HT – hyperthermia treatment

HyD – hybrid detector, combination of the vacuum tube technology with the avalanche technology

IR – infrared

LP700 – long-pass optical filter with the cut-off wavelength of 700 nm

MDR – multidrug resistance

MP – multi-photon

MWHT – microwave-induced hyperthermia treatment (sometimes referred to in a simpler way as a microwave hyperthermia treatment)

NDD – non-descanned detection or non-descanned detector

NIR – near-infrared light

NR – Nile Red

PMT – photomultiplier tube

PSF – point spread function

QMLE – quick maximum likelihood estimation

RCM – reflectance confocal microscopy

RT – room temperature

S. cerevisiae – *Saccharomyces cerevisiae*

SHG – second-harmonic generation

SHIM – second harmonic imaging

SP700 – short-pass optical filter with specific cut-off wavelength (700 nm)

STED – stimulated emission depletion microscopy

TEM – transmission electron microscopy

UV – ultraviolet light

WD – free working distance

Introduction

Light microscopy served as a tool for learning the microworld since centuries. As technology developed, different imaging methods were invented and implemented first as unique equipment, becoming later on a routine tool for everyday usage. Modern laser technology, electronics and computers enabled numerous advanced microscopic methods, in particular workhorses of cell and molecular biology – confocal and two-photon excitation microscopy for studies of both dynamical processes and 3D structures including mutual arrangements of different microscopic objects.

During the last two decades it seemed that technology came to it's edge, reaching the theoretical resolution limit for light microscopy (which is approximately half a wavelength of the light used for the image formation [1], [2], [3], [4]) and progress was focused on faster image acquisition (reaching video frame rate [5], [6], [7], [8]) as well as development of advanced data acquisition techniques, e.g. FRAP, FLIP, FRET, FLIM, FCS and a number of others.

Development of a variety of optical microscopic techniques is based on ongoing fast improvement as to the technical advances (new and/or improved HW components, etc.) as well as the ever broadening scope of their applications. It is important to exploit the new possibilities correctly and efficiently, enabling not only visualization of microscopic structures of interest, but also their analysis in a reproducible way. Keeping in mind the recognition of technological progress in super-resolution light microscopy by the Nobel Prize in chemistry (2014), it would be no exaggeration to say that we can expect many interesting findings and exciting discoveries in molecular and cell biology. So, nowadays we are witnessing the renaissance of the light microscopy, especially after recent surpassing the diffraction limit, which seemed to be the unbeatable physical limitation [9], [10], [11], [12], [13], [14], [15], [16], [17].

Aims of the study

Each technique addressing a certain problem which was not solved so far, is important. Quite often, quantitative improvements open the door to qualitative discoveries and serve as a tool for broadening knowledge about the surrounding world in the finest details.

The aim of this study was to develop methods and approaches for image acquisition with subsequent image analysis of image data, obtained by confocal and two-photon excitation microscopy as well as their combination, enabling new possibilities of visualization and assessment of information on biological tissues and cell structures in 3D and their measurement. We focused on methods that exploited advantages of confocal and multi-photon excitation microscopy. Our further aim was to demonstrate the applicability of non-invasive approach for in vivo applications, usefullness and the relevance of these methods in several special biological applications with emphasis on improved image acquisition, analysis and evaluation of real biological samples.

Literature overview

Microscopes serve as a visualization tool for several centuries, first references ascend to the end of 16th century (Jansen's microscope [18], [19]); the first confirmed publication which contained the microscopic images is dated 1630 [20]. Shortly thereafter, systematic observations [21], [22] and the recognition of another systematic study by the Royal Society in London followed [23]. It is hard to mention all contributors to the development of theory, design and reproducible manufacturing of the optical devices. However, one can hardly overestimate the significance of Ernst Abbe's research on image formation and lens aberrations [1], introduction of fluorescent microscopy concept [24], [25] (backed up with immunofluorescence [26], [27] and later on – by fluorescent proteins as a markers for gene expression [28]), phase contrast [29], [30], differential-interference contrast [5], [6], [31], [32], [33], total internal reflection microscopy – TIRF [34], [35], [36], [37] as well as confocal microscopy [38], [39], [40], [41], [42], [43], [44], [45], [46] and two-photon excitation microscopy [47], [48].

When the light used for exciting fluorophores is focused onto specimen, the maximum excitation rate is at the focus point. Subsequently, the maximum of fluorescence intensity comes from this region. On the other hand, fluorescence is also excited in the points lying above and below the focal plane. In order to get rid of the light originating from planes different from the focal one, the confocal pinhole can be introduced. It lies in optically conjugated focal (con-focal) plane and prevents the out-of-focus light to pass to the detector placed behind the pinhole; thus, most of the recorded signal comes from the focal point.

Due to the fact that most of the emission is filtered out by a confocal pinhole, higher excitation light intensities as well as sensitive single-point detector are required to get a reasonable signal-to-noise ratio.

As excitation sources with higher light intensity and brilliance, sensitive detectors (photomultipliers, avalanche photodiodes, gallium arsenide phosphide – GaAsP and hybrid detectors – HyD) as well as fast control electronics and computers became

available, several implementations of confocal laser scanning microscope were introduced for true 3D image data acquisition in late 1970s [49], [50], [51], [52].

Confocal laser scanning microscopy (CLSM)

The confocal laser scanning microscopy (CLSM) exploits the advantages of fluorescence microscopy. Essentially CLSM concept is based on the usage of the aperture and confocal pinholes. The former provides that a sample is illuminated by a point-like source of excitation light; both are placed in (physically different) planes optically conjugated to object plane. The confocal pinhole passes all light originating from the focal point situated within a sample (where the image of an aperture pinhole is created by the objective) and most of the light coming from the planes directly adjacent to the focal one. Also, only a small portion of light form optical planes further apart would get through the confocal pinhole and will be registered by a single-point detector placed directly behind the pinhole. Therefore, the detected signal would essentially consist of the light coming from the focal point, whereas contribution of a signal from points above and below the focal plane would be neglectable (nevertheless, non-zero). It is noteworthy that only the signal from one single point can be registered at once. In order to get a 2D image, the sample is scanned laterally point by point either a) by moving the specimen [53], or b) by moving the confocal spot over the specimen by means of tiltable mirrors [54], [55] or c) scanning the sample by a moving pinhole (or array of pinholes) as it is realized in Nipkow spinning disk microscopes (or improved by microlenses in Yokogawa design) with registration by 2D position-sensitive detector, e.g. CCD camera [56]. Finally, for collecting 3D information about the object (and building up 3D virtual model), the position of focal plane is moved across the sample either by changing the position of sample stage or objective.
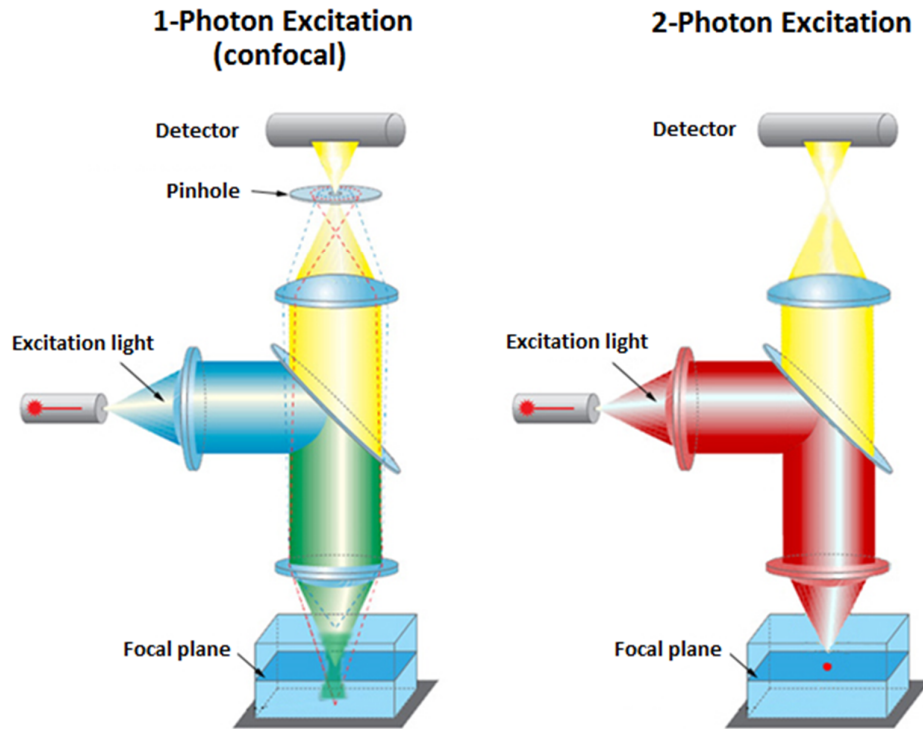
Figure 1. Comparison of confocal (left) and two-photon excitation (right) microscopy principles (adapted from [57]). In confocal (1PE) microscope, the pinhole in the plane optically conjugated to the focal one is responsible for the optical sectioning capabilities. In case of two-photon excitation (2PE) microscopy, excitation only occurs in a focal point, possessing therefore intrinsic optical sectioning properties, and confocal pinhole is no needed (in practice – is fully open).

Reflectance confocal microscopy

In the reflectance confocal microscopy (RCM), the reflected light is detected by a confocal (descanned) detector. In practice, it utilizes the settings of confocal microscope hardware so that the backscattered light with the same wavelength as excitation light source is registered. Reported as "confocal histology", it was applied to normal skin, vitiliginous skin, and a compound nevus [58]. After improving this technique [59], it was considered that it has a high potential for in vivo diagnosis [60], [61]. In comparison withthe golden standard – histopathological examination, the RCM enables quick and painless skin visualization *in vivo* with no artifacts due to the skin alterations by the procedure itself. Therefore, the image acquisition can be

performed systematically, thus improving the performance of the applied treatment for each patient individually.

Later on, RCM was applied for studies of melanoma and non-melanoma skin cancer, inflammatory skin diseases [62]. The RCM approach was also used in endoscopy [63], [64] as well as ophthalmology [65], [66].

It can be concluded that RCM is a promising tool for diagnostics and monitoring of inflammatory lesions, melanoma and other skin cancer and diseases.

Two-photon excitation microscopy

The idea that two photons can combine their energies to cause the sum-up effect was mentioned in 1905 [67]. In 1931, the quantum mechanical formulation of two-photon excitation (2PE) was reported [68]. In such process, an electron is excited by simultaneous absorption of two photons having exactly the half of energy, necessary for such electron transition (Figure 2). To achieve UV or visible 1PE, the wavelength for 2PE must be in the red or near-infrared spectral range (700-1600 nm).
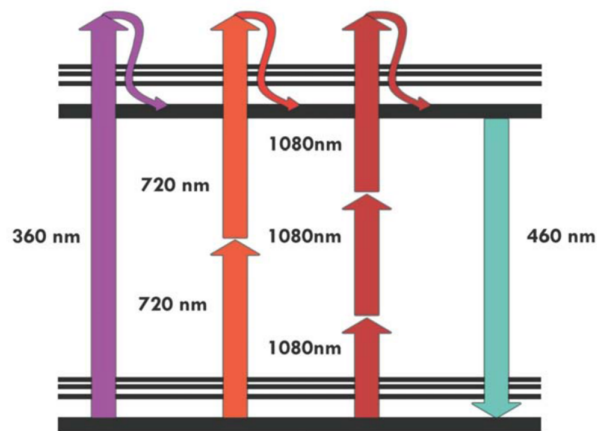

Figure 2. Simplified Perrin-Jablonsky diagram for one-, two- and three-photon excitation, resulting in fluorescence with the very same wavelength [69]. The rule of thumb is that one can use multiple wavelengths with respect to the one-photon excitation condition accordingly with the *n*-th photon excitation order. Optimization can be obtained at different wavelengths.

For the first time 2PE was experimentally observed on $CaF_2:Eu^{2+}$ crystal by Kaiser and Garret in 1963 [70] and realized first with dye laser [47], and, later on, with femtosecond Ti:sapphire mode-locked laser [48].

The probability of 2PE is much smaller compared to 1PE case. For instance, a rhodamine B molecule (an excellent 1- or 2-photon absorber) absorbs a photon through a 1-photon process about once a second in bright sunlight, while it would absorb a photon pair in 2PE event every 10 million years [71]. In order not to wait for 2PE event for centuries, one needs to substantially increase the number of incident photons in time-space quantum volume. To do so, it is necessary to provide a huge amount of photons concentrated to as small volume as possible (the required photon flux typically 10^{20}-10^{30} photons/(cm^2 s) [72]). For this purpose, high-power infrared laser light is focused by an objective with high numerical aperture. The light is focused on a diffraction-limited spot 0.5 µm in diameter, i.e., on area of $2 \cdot 10^{-9}$ cm^2, resulting in average power in the spot of $5 \cdot 10^7$ $W \cdot cm^{-2}$. So, when laser is on, instantaneous power reaches $5 \cdot 10^{12}$ $W \cdot cm^{-2}$. Considering the power of a typical nuclear reactor to be 10^9 W, the peak energy density at the specimen during each pulse is equivalent to the output of 5000 nuclear reactors converted to light and focused on a square centimeter. In order to decrease the laser damage of a specimen, the pulsed lasers are used, providing 100 fs pulses every 10 ns (pulse duration to gap ratio $\sim 10^5$) as depicted in Figure 3. Therefore, the average laser power is relatively low (of order of 100 mW) and not much greater than for a conventional confocal microscope [73], thus causing low or no damage to the specimen under investigation. It was shown that the 2PE image acquisition was gentler than that by conventional confocal approach (i.e. 1PE) [74], [75].

Provided the above mentioned conditions are satisfied, the 2PE event can only occur in the confocal focus, since it depends on the square of light intensity. The excitation probability is non-zero only within a tiny volume (order of 1 fl, or 1 µm^3). Therefore, all photons with wavelength in the range expected for emitted fluorescence are considered to be originating from the confocal point (Figure 4). Due to this intrinsic optical sectioning capability (i.e., atoms can be excited and, therefore, fluorescence can occur exclusively in confocal point), there is no need for a confocal pinhole in the case of 2PE fluorescence imaging [76]. Another consequence of single-point excitation is reduced photobleaching by limiting it to the focal plane of

the microscope, since the fluorescent molecules within the specimen are not excited unless they are in focus (Figure 5) [47], [77], although increased photobleaching was reported due to higher-order resonance absorption effects [78]. Due to higher viability of biological objects, the observations of living cells are possible over extended period of time. The 2PE imaging experiments on living cells and even organisms were reported [79], [80].
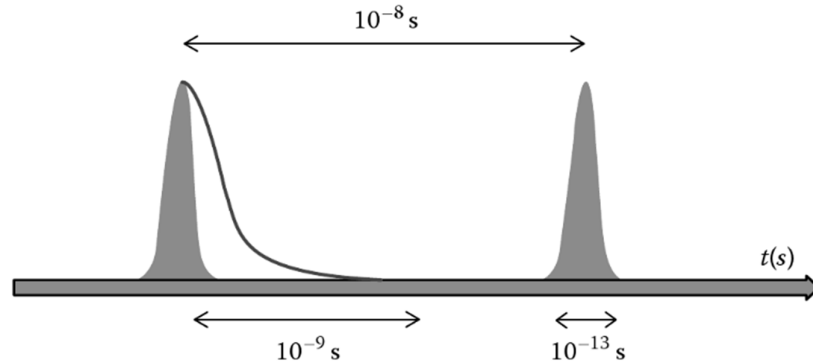
Figure 3. Illumination laser pulse duration, pulse repetition rate, and fluorescence decay (not to scale), from [81]. The laser is on for the very small fraction of time (~0.01% of the image acquisition time). The frequency of laser pulsing is optimized in accordance with the typical fluorescence decay.

Usually, IR laser sources are coupled to confocal microscopes with one-photon excitation with embedded pinhole [82]. Therefore, in the case of 2PE a pinhole is set to a maximum (fully open) in order to record as much useful signal as possible. In order to improve the signal-to-noise ratio, non-descanned (ND) mode is used. In this mode, the detector block (e.g., from two to four detectors along with filter cubes for certain wavelengths) is situated directly after the objective. In such configuration, the desired signal does not pass back through the galvo scanning mirrors and a pinhole, thus improving the signal-to-noise ratio and providing detection of the weaker signal coming from deeper layers of the sample [83].

Typically, the laser source consists of a Ti:sapphire pulsed pumped by Ar ion or solid state diode laser. The wavelength of output light is tunable (from 690-720 nm up to 960-1090 nm); the repetition rate is 76-80 MHz (i.e. pulses follow every 12.5 – 13.2 ns) and the pulse duration is 110-140 fs. For image acquisition,

a 20x – 100x objectives with numerical aperture 0.7-1.46 can be used. From this point of view, the oil immersion is preferable, since water evaporates considerably from both coverslip surfaces due to direct contact with a specimen being heated up noticeably by high-power IR light. This might be a problem for long time-lapse measurements with water immersion objectives. However, it can be overcome e.g., by utilizing the immersion oil with the refractive index close to water or live-cell incubator with embedded humidifier covering the microscope stage. For deep tissue imaging, the water immersion objectives perform much better due to lower refractive index mismatch. In case of oil immersion, the PSF size is increased by a factor of 2 for depth of 50 µm (and getting even worse for deeper sections), significantly reducing the 2PE efficiency and, subsequently, the fluorescence signal intensity as well as spatial resolution. At the same time, when the water immersion objective is used, the changes in PSF size and fluorescence intensity are very small and do not exceed 10% [84].

The multi-photon excitation spectra can hardly be estimated from one-photon data because of different cross-sections, selection rules and the distinct effects of vibronic coupling [85]. Usually, doubling the known one-photon excitation wavelength can be used as a good first approach. However, the difference can be as big as 100 nm, e.g. for rhodamine 123, or even 200 nm, e.g. for SNARF-1 [86]. On the other hand, 2PE absorption spectra are broader than those for ordinary one-photon excitation. Therefore, two [87], three [80], [88] or even four [89] different fluorescent dyes can be excited simultaneously by single 2PE wavelength. The latter fact might cause problems with emission spectra overlapping, so special attention is necessary in order to get rid of such cross-talk.
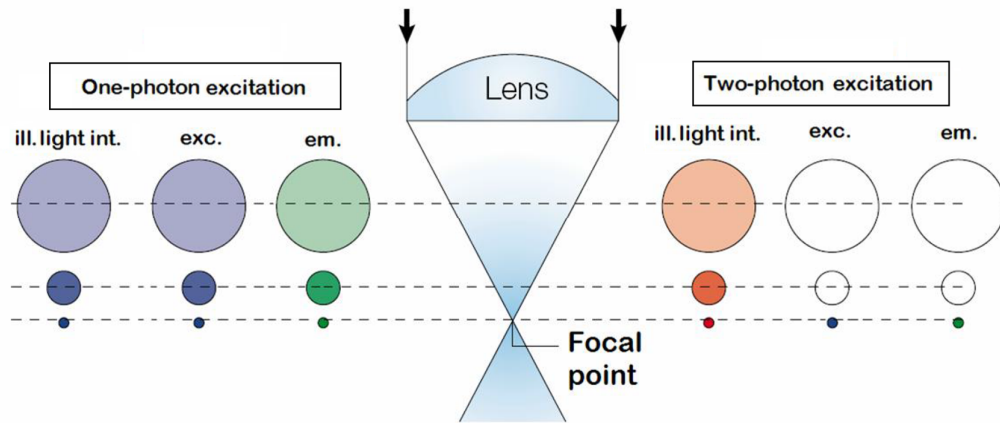
Figure 4. Comparison of illumination light intensity (*ill. light int.*), probability of excitation (*exc.*) and emission intensity (*em.*) of a fluorophore in different planes in the case of one-photon excitation (1PE, left) and two-photon excitation (2PE, right), applied to a fluorophore in homogenous solution. (Modified from [73]).

At the same time, there is no difference in emission spectra in the case of 1PE and 2PE [85], since the fluorophores' emission spectra depend exclusively on electron structure of the particular fluorophore molecule (Figure 2). However, authors of the latter paper [85] reported a considerable red shift and also a tendency for the shifted 2PE maxima to coincide with side maxima of the 1PE spectra [86].

Main advantages of 2PE microscopy:

1) the near-infrared light (with wavelengths just above the approximate end of the response of the human eye up to the absorption band of water molecules – from 750nm to 1.4 µm) suffers from significantly less absorption in biological specimens compared to UV and visible light; the scattering of NIR light is also reduced since scattering decreases with increasing the wavelength [90], so it is particularly suited for imaging in optically thick specimens;
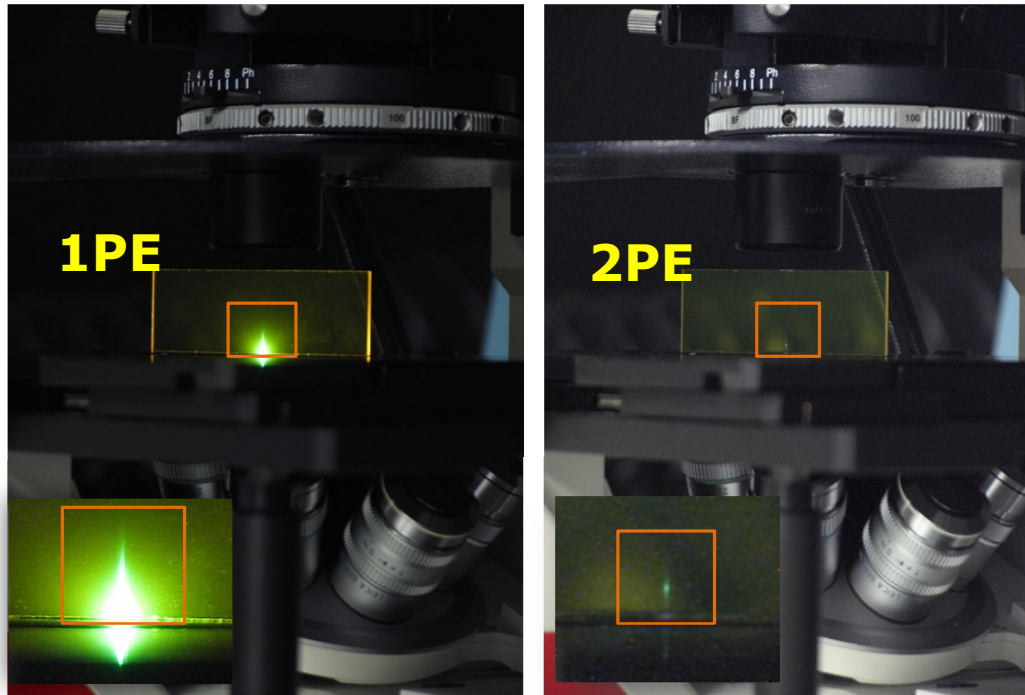
Figure 5. An experiment to illustrate the difference between ordinary (single-photon) excitation of fluorescence and two-photon excitation (experimental design – after [72]) realized at Leica SP2 AOBS MP on piece of fluorescent plastic (Chroma Technology Corp.). The 488nm excitation by Ar ion laser was used for 1PE (left). The lower half of the double cone is clearly seen, the upper part is faded due to scattering. For 2PE (right) the 860 nm of Chameleon Ultra IR pulsed laser (Coherent, Inc.) has been used. The emission confined to a tiny volume is clearly seen. There is no emission observed from planes above and below the focal one.

2) inherent optical sectioning capability – fluorophores are excited in a limited volume only, therefore no pinhole is needed (or can be fully open), providing that all emitted photons hitting the detector contribute to the image formation since they are not rejected by the fully open confocal pinhole; also, for the same reason there is no increased background due to fluorescence occurring outside the focal point caused by the absorption of scattered photons of illumination light as it is in 1PE case [91];

3) there is lower photobleaching (due to the confined excitation volume) and photodamage (due to the lower absorption of NIR by specimen) compared with confocal (1PE) case, when the whole double-cone is excited above and below the focal plane;

4) due to broad 2PE spectra of fluorophores it is possible to excite more fluorescent dyes at once by means of the single 2PE wavelength, which allows multicolor imaging (simultaneous in several spectral channels) with one IR laser with no need of tuning it to another excitation wavelength;

5) wide gap between excitation and emission makes it easier to reject excitation light with minimal loss of emission photons;

6) not only confined excitation volume decreases photobleaching, but also enables localized photochemical reactions to take place, e.g. chemical photoactivation [92] or 3D FRAP [93].
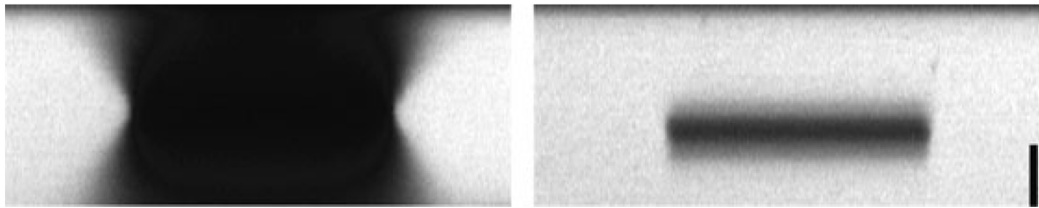
Figure 6. The consequence of intrinsic optical sectioning capabilities for two-photon excitation microscopy (2PE): axial photobleaching patterns produced by conventional confocal and two-photon excitation after imaging a single plane inside a polymer film containing sulforhodamine B. On the left, the effect of conventional confocal illumination (514 nm); on the right, the effect of two-photon illumination (820 nm). Scale bar 5 µm [94].

On the other hand, there are also significant disadvantages of this technique. These are

1) slightly worse spatial resolution due to the longer wavelengths used (as a result of interplay between longer excitation wavelengths and localized volume where excitation occurs due to quadratic dependency on illumination intensity);

2) potentially higher photodamage in case the specimen contains chromophores that absorb the excitation wavelengths;

3) two-photon excitation spectra are still very complicated to be predicted theoretically, and far not all fluorophores are fully characterized for 2PE;

4) lower image acquisition speed in comparing to 1PE confocal approach;

5) very expensive setup.

Depending on the properties of the tissue (and the exact definition of imaging depth) 2PE microscopy can image up to 1 mm in tissue [95], [96], in vivo imaging up to 1.5 mm deep into brain tissue was reported for excitation wavelength of 1275 nm [97], [98]. Although this is impressive compared to other high-resolution techniques, this depth still covers only a small fraction of the mammalian brain. The imaging depth is determined by scattering: with increasing depth, a smaller fraction of the incidence photons are delivered to the focus [99].

The successful studies on functional imaging of neurons [100], 3D in situ imaging of cellular metabolic redox in cornea [101], dermatological studies [102], lifetime imaging of cells autofluorescence [103], [103] [104] as well as 2PE applications to immune system studies [105] are reported. Besides, techniques based on 2PE tomography and microendoscopy can provide clinicians and researchers with high-resolution in vivo optical biopsies based on two-photon autofluorescence, SHG, and FLIM data which are important for early stage melanoma detection, skin aging, in situ screening of pharmaceutical and cosmetical products [106].

Second Harmonic Generation (SHG)

For centuries, humankind dealt with incoherent light with relatively low intensities. In such conditions the response of medium to light is linear. Consequently, there were no needs to take into account non-linear effects. Invention of lasers in 1960s made high enough light power level available in laboratories. It was observed that the optical response depends on the light intensity, which led to development of a new field of non-linear optics with various intriguing phenomena, such as second harmonic generation (SHG).

The atom interaction with light is described by a classical oscillator model. When the electric field intensity of incident light wave is small compared to intra-atomic forces (determining the bonding energy), the atomic oscillator response is linear. However, when increasing the intensity of light (e.g., in laser beam of high power),

the medium response becomes non-linear due to anharmonicity of atomic oscillator. The best known effect is SHG due to non-linear dependence of polarization on the electric field intensity of incident light, when the higher power terms of the expansion should be taken into account.

The barium niobate glass is an example of non-linear optical medium, where SHG is possible. For instance, while incident light with a wavelength of 1060 nm goes through an optically transparent crystal of barium niobate, it is converted into light with exactly the half of original wavelength, i.e., 530 nm. Collagen is an example of biological material visualized by SHG.

The SHG peak is sharp. Thus, while utilizing SHG along with 2PE fluorescence imaging, these two signals can be easily distinguished with slightly changing wavelength of the IR laser source used for two-photon excitation. In this case, the emission spectrum remains unchanged (the emission peak shape does not depend on the excitation wavelength; also, two-photon excitation spectra are rather broad, and small wavelength change in excitation light does not influence the emission intensity neither), whereas the SHG signal disappears (if the detection range was set narrow enough). At the same time, it should appear for appropriate 2PE wavelength (usually set to the transmission window of corresponding filter in modern easily tunable IR pulsed lasers).

Another feature of SHG, the emitted light is coherent and therefore must satisfy phase matching constraints. For example, the SHG profile in MPM retains phase information and emits with directionality dependent on the nature of the scatterers [107], [108], whereas fluorescence emission is isotropic.

Due to intrinsic property of SHG ability, SHG imaging does not require any staining; collagen is a good source by itself [83], [109], [110], [111]; signal intensity is proportional to collagen concentration. SHG has directional emission, and depends on molecular arrangement. Also, there is no photobleaching. Thus, observing SHG signal can be considered as non-invasive technique, which allows observation of living tissues. Also, it is applicable to myosin fibers as well as other dipolar proteins, such as microtubule arrays [110], [112], [113].

The observation of SHG was reported in 1961 [114], but it took several years to implement this phenomenon in a variety of interfacial studies, including liquid-solid, liquid-air, and liquid-liquid interfaces [115] as well as to spectroscopy [116], [117]. Many of the approaches used to probe bulk interfacial properties can be extended to microscopy. This idea was first demonstrated in the 1970s by Hellwarth and Christensen [116] and Sheppard [50], [118], [119], [120]. First biologically relevant study by SHG imaging (SHIM) experiments were reported by Freund and colleagues on a rat-tail tendon in 1986 [109].

The application of SHG to microscopy including necessary changes to two-photon excitation microscope configuration was described e.g. in [79].

Because of the interfacial specificity of the process, SHG is an ideal approach to the study of biophysics in model membranes [121], [122] and the membrane physiology of living cells [123], [124], [125].

Since then, more SHG applications on unstained specimens were reported [126], [127], especially useful they were in tissue studies [128], [129], [130], and collagen visualization [131], [132], [133], [134].

The 2PE fluorescence and SHG microscopy can be easily implemented simultaneously, while providing complementary information on tissue structure due to different contrast mechanisms. Recently, the combination of these two imaging modalities has been proved to be useful in examination of skin [110], [135] and other tissues [113], [136], [137], [138], [139], [140], [141]. On the other hand, the combination of imaging modalities based on 1PE and 2PE is still used very rarely [135], [142], although it could bring a complex information on appearance and arrangement of fresh tissues.

Implementing the above microscopy techniques into the *in vivo* as well as *ex vivo* experimental cancer examination could be well exploited in clinical applications, mainly skin pathologies. However, in studies of experimental melanoma in mouse or rat only 1PE based techniques [143], [144] and SHG imaging [145] separately were applied. Our idea was that the combination of 1PE and 2PE microscopy could shed more light on relationships between different types of tissues, thus being of a significant diagnostic value in cancer research. The above microscopy techniques

could be especially useful in studies of changes in tissue morphology after different clinical interventions, such as treatments with locally induced hyperthermia (HT). The use of heat to provoke tissue damage as an anticancer treatment was demonstrated to be therapeutic for enhancing the curative effect of other anticancer treatments (chemotherapy, radiation therapy) [146].

Image postprocessing

Images acquired by means of any optical system are only a representation of the investigated objects. It is due to the fact that any optical system is imperfect and there is inevitable quality degradation due to diffraction and noise. Also, optical faults, (such as chromatic and / or spherical aberrations due to objective imperfection, sample preparation issues, wrong coverslip thickness and immersion medium) as well as acquisition errors (undersampling, clipping, digitization artifacts, scan artifacts, mechanical and / or illumination instability) impair the image quality. Fortunately, these can be partially compensated for or even fully excluded by correct choice of the equipment and image acquisition settings. The process of recovering the real object from acquired images based on theoretical or experimental knowledge of how the instrument degrades the image (optical transfer function) is called deconvolution.

The deconvolution essentially re-assigns the registered light intensities spatially, thus improving the contrast and the resolution of acquired images. This procedure can be applied for single images and stacks acquired by wide-field, confocal [147], [148], two-photon excitation microscopy [149] as well as for STED [150] or digital holographic microscopy [151].

Experimental Set-up and Techniques

In our studies we used microscopic set-up and techniques described below.

Microscope, excitation sources and detectors

All presented data were obtained on commercially available confocal laser scanning microscope Leica SP2 AOBS MP with acousto-optical beam splitter (AOBS) based on a Leica DM IRE2 inverted microscope and equipped with an argon laser (458 nm/5 mW, 476 nm/ 5 mW, 488 nm/20 mW, 514 nm/20 mW) as well as two HeNe lasers: green (543 nm/1.2 mW) and red one (633 nm/10 mW) used for 1PE experiments. For 2PE excitation, we used a mode-locked Ti:Sapphire Chameleon Ultra laser (Coherent Inc., Santa Clara, CA, USA), tunable from 690 nm to 1040 nm with the pulse width of 140 fs, coupled to the confocal scanning head of the microscope. For the acquisition of relatively large field of view, an HC PL FLUOTAR 5x dry objective with a WD of 12.2 mm and an NA of 0.15 or an HC PL APO CS 10x dry planapochromat objective (WD = 2.2 mm, NA = 0.40) were used. In most cases we used an HC PL APO CS 20x water immersion planapochromat objective (WD = 250 μm, NA = 0.7), often yielding sufficient resolution while offering a relatively large field of view. For imaging cell details we used an HCX PL APO CS 63x water immersion planapochromat objective (WD = 220 μm, NA = 1.2). When the highest possible resolution was required, the HCX PL APO CS 100x NA = 1.4 oil immersion objective (WD = 90 μm) was used.

The experimental setup of image acquisition is shown for the special case of melanoma imaging in Figure 7. The previously exposed tumor was directly placed on the cover slip glass, and maintained humid by drops of the same liquid used for the microscope objective (in most cases we used water with water immersion objective). Thus, the damage by drying was avoided, more homogeneous adhesion to the glass was achieved, and possible optical aberrations were reduced. A similar procedure was applied for imaging the subcutaneous side of the skin flap, which was used as a control, and for the fresh samples.
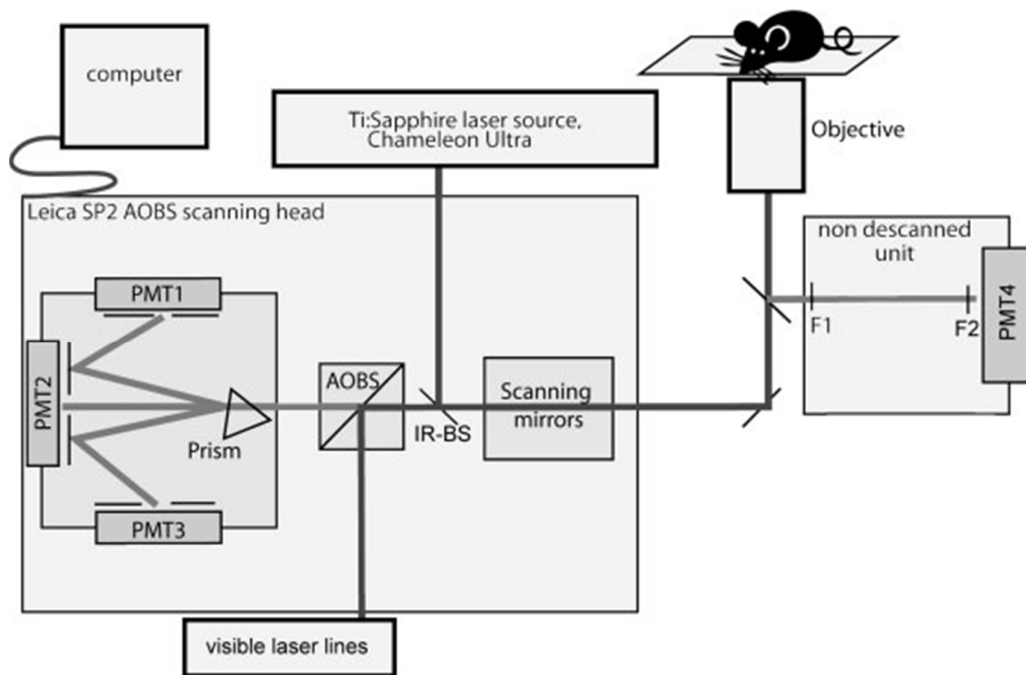
Figure 7. Schematic view of experimental setup. Confocal laser scanning microscope Leica SP2 AOBS was coupled with IR-pulsed laser Chameleon Ultra for two-photon excitation. In the presented setup, the living mouse, under general anesthesia, lays on a cover slip glass placed on the stage of the inverted microscope, with the tumor exposed by dissecting and removing a skin flap.

The fluorescence, autofluorescence and SHG signal were detected by

i) 3-channel descanned confocal detector with flexibly tunable spectral detection, often by simultaneous multichannel detection of spectrally resolved fluorescence;

ii) non-descanned PMT detector; in most cases – by single spectral channel detection of the signal with LP700 and BP430/24 (Chroma Technology Corporation) optical filters for the SHG signal with IR pulsed laser Chameleon Ultra at 860 nm, in some cases – by simultaneous 2-channel detection of the spectrally resolved fluorescence signal by the standard Leica filtercube with SP700 dichroic mirror and BP525/50 and BP610/75 band-pass emission filters used for green and red light detection respectively.

Image acquisition modes

One-photon excited fluorescence and autofluorescence

One-photon excited (1PE) fluorescence and autofluorescence imaging was performed using conventional for confocal microscopy approach. We examined the vasculature in the experimental melanoma capsule in living mouse with vessels stained by intracardially injected FITC-dextran. We used FITC-dextran 150 kDa because its large molecular weight was impeding the diffusion of the molecules from the vessels into the surrounding tissues. The wavelength of 488 nm was used for excitation and the wavelength range from 500 to 560 nm for detection.

Confocal reflectance mode

The images in reflectance mode were acquired by using excitation wavelengths of 488, 514, and 633 nm. The reflected signal was detected in up to three corresponding channels simultaneously, using detection wavelength range of 478-498, 504-524, or 623-643 nm, respectively with AOBS set to maximum detection of reflected light. Each of the three different excitation wavelengths applied in reflection mode was valuable and brought specific information due to its specific scattering behavior. The choice of three spectral lines (blue, green and red) was supposed to bring color information in confocal mode, resembling to a certain extent the natural basis for a color perception. Indeed, information from different channels was mutually complimentary, thus increasing image contrast (for different parts of field of view different channels were useful).

For the 2PE fluorescence and autofluorescence the following approaches were used. The two-photon fluorescence signal was usually collected in descanned (D) mode, i.e. via internal detectors placed inside the scanning head behind the pinhole. Depending on the specimen, one-channel detection or simultaneous detection of two spectral channels by two activated detectors was performed. The flexible spectral detection window was set in accordance to the fluorophores' emission spectra. We applied different wavelength ranges, usually optimized using lambda scans to get as strong autofluorescence signal of the tissues as possible. In some cases, when the GFP signal was too weak for proper detection in D mode, we applied 2PE in non-descanned (ND) mode, using an external two channel detector. In this way we could get an improved signal-to-noise ratio in the acquired images. In ND configuration, the external detector (PMT4 in Figure 7.) was placed behind a 700 nm short pass filter (F1) to remove reflected light of wavelengths over 700 nm, preventing detector damage by reflected high power IR light, followed by a 525 nm band pass filter (F2) with a bandwidth of 50 nm. This setting improved detection of the GFP signal; however, we found that the ND configuration using a narrow red bandpass filter was not optimal for the detection of BCP, therefore the BCP signal was acquired in D mode, using a wide detection range from 600 to 750 nm.

Using the above microscope settings, we acquired either images of individual optical sections in different layers of colonies, or 20–50 mm thick stacks of a series of optical sections (z-series), usually 2.5–3.5 mm apart. For noise reduction, we applied line or frame averaging during the acquisition of images. To compensate for light attenuation with depth, which is common in confocal and 2PE microscopy [152] and which we often encountered during the acquisition of the z-series of colonies, we usually used the Intensity Compensation feature of Leica Confocal Software, Version 2.61 (Leica Microsystems Heidelberg GmbH) in 'Linear by Gain' mode [153].

An overview of the morphology of colonies and individual cells was obtained simultaneously with green fluorescence as autofluorescence in the 600-740 nm wavelength range. Images of colonies older than 2 days were composed of two or three stitched fields of view [154].

For investigation of structures generating SHG signal, especially fibers containing fibrillar collagen, we used 2PE at the wavelength of 860 nm, which implied expected detection of SHG signal at the wavelength of 430 nm. Back-scattered SHG signal is reported to be 16 to 20 times weaker than forward-scattered one [133]. However, in present study it was impossible to detect SHG signal in forward direction on live animals and relatively thick skin flaps. On the other hand, for simple visualization and measurement of fiber lengths and comparison of relative intensities [83], SHG imaging via the backward channel was sufficient.

For SHG imaging, we used descanned or nondescanned mode. In a descanned mode, SHG was recorded through the confocal scanning head in the detection range 420-440 nm (PMT1) while excited with 860 nm of IR pulsed laser Chameleon Ultra (Coherent Inc). In a nondescanned mode, the light was collected directly behind the objective by PMT4 after passing through E700SP short pass filter (F1) followed by a 430DF15 band pass filter (F2), providing SHG signal when IR laser wavelength of 860 nm was used. To confirm the detection of SHG signal, we checked if the signal disappeared when the excitation wavelength was changed to 800 nm, and then re-appeared after setting the flexible detection window to 390-410 nm (D mode) or setting up a band pass filter for 400 nm (ND mode). Since the laser power is not constant for different wavelengths, it was not possible to filter out the autofluorescence by subtracting images acquired with SHG signal present and filtered out.

Typical averaged laser output power (measured at the exit pupil of the Chameleon Ultra laser) was around 3 W. Average laser power at the sample space was measured with objective removed from the optical beampath by the highly-sensitive thermopile sensor PM3 (for wavelength range 300-1100 nm and maximum measured power 2 W) placed at the sample space and connected to laser power meter FieldMaxII (Coherent Inc.) and subsequently normalized by the objective transmission data provided by Leica Microsystems GmbH. In laser power measurements, we kept the system settings same as during the acquisition of our images. Typical values of the averaged laser power did not exceed 120 µW for 1PE and 100 mW for 2PE (see Table 2 in [155]). These data can be directly

compared to standard values certified by Leica Microsystems (measured at the sample space with objective 10x Dry NA 0.4 with zoom set to maximum and all internal shutters open during the scan) by simple re-normalization.

Settings for particular specimens are described in details in original publications.

Image postprocessing

For deconvolution, the Huygens Professional software package (Scientific Volume Imaging, Hilversum, Netherlands) was used. Stacks of images were deconvolved using 'quick maximum likelihood estimation' (QMLE) algorithm using the experimental PSF. For this purpose, the 3D confocal stacks of fluorescent microbeads were acquired at the same imaging conditions as images to be deconvolved, and these data were used as an experimental PSF for deconvolution procedure. The image processing algorithms and 3D visualizations was performed, e.g., in Ellipse (ViDiTo, Slovakia, www.ellipse.sk) software environment using our custom-made plug-in modules (Smooth3D, Thresh, Surface by RNDr. Jiří Janáček, PhD). The granularity measurements were performed using Smooth, Lipschitz, and MeasureThres modules (by RNDr. Jiří Janáček, PhD) developed in Ellipse3D software environment.

Also, some other image processing and visualization software packages were used, such as tools for visualization and comprehensive image data analysis Fiji [156] based on ImageJ [157], [158], [154].

Comments on presented publications

The present work was not oriented on just one specific biological problem, but rather to methodological contribution to several types of biological problems. As a result, several advanced image acquisition modes were developed. Also, these approaches were tested on several different biological objects. Several research projects benefited substantially, and results were published in impacted international journals.

Architecture of developing multicellular yeast colony: spatio-temporal expression of Ato1p ammonium exporter

Libuše Váchová, Oleksandr Chernyavskiy, Dita Strachotová, Paolo Bianchini, Zuzana Burdíková, Ivana Ferčíková, Lucie Kubínová, Zdena Palková, Environmental Microbiology **11** (7) (2009), 1866–1877.

Yeasts, when growing on solid surfaces, form organized multicellular structures, colonies, in which cells differentiate and thus possess different functions and undergo dissimilar fate. Understanding principles involved in the formation of these structures requires new approaches that allow the study of individual cells directly in situ without needing to remove them from the microbial community. Confocal microscopy was considered as a suitable technique for these studies.

When developing a proper application of confocal microscopic technique, the main problem was connected with the rather low penetration depth of the laser beam into the colony, due to the low transparency of yeast cells covered by optically dense cell wall. This caused a rapid decrease of the detected signal intensity in deeper cell layers, which became the main limiting factor of the *in situ* usage of confocal microscopy approach.

We supposed that two approaches – from the top (top-view) or from the bottom (bottom-view) of the yeast colony would allow us to analyze the deeper layers.

Surprisingly, the top and bottom confocal microscopy scanning gave a completely different picture. To complete the view of the colony we prepared a sample of the vertical section of the microcolony by cutting it down the middle. This sample scanned with 2PE revealed a side-view of the microcolony.

In contrast to 1PE confocal microscopy, which only allowed us to observe the outermost surface cell layer of the yeast, the 2PE approach enabled us to also obtain a fluorescent signal from several internal layers without damaging the cells. In all experiments described in this paper, we therefore focused exclusively on the 2PE confocal microscopy approach.

The new approach enabled us to monitor the presence and spatial location of fluorescently labelled proteins as well as structures stained with specific fluorescent dyes within *S. cerevisiae* microcolonies by use of two-photon excitation (2PE) confocal microscopy. The new technique allowed us to reveal spatial location of cells producing the transmembrane protein Ato1p within developing yeast microcolonies. Moreover, we show how the Ato1p production pattern can be influenced by colony development or by the presence of neighbouring colonies. In addition, we show that cells located in surface layer of *S. cerevisiae* microcolonies are tightly joined via thick cell wall and form a thin protective cell layer which blocks penetration of harmful compounds. The cells forming the layer are tightly connected via cell walls, the presence of which is essential for keeping protective layer function. Viewing the colonies from different angles allowed us to reconstruct a three-dimensional profile of the cells producing ammonium exporter Ato1p within developing microcolonies growing either as individuals or within a group of microcolonies. We show that neighbouring microcolonies coordinate production of Ato1p-GFP. Ato1p itself appears synchronously in cells, which do not originate from the same ancestor, but occupy specific position within the colony.
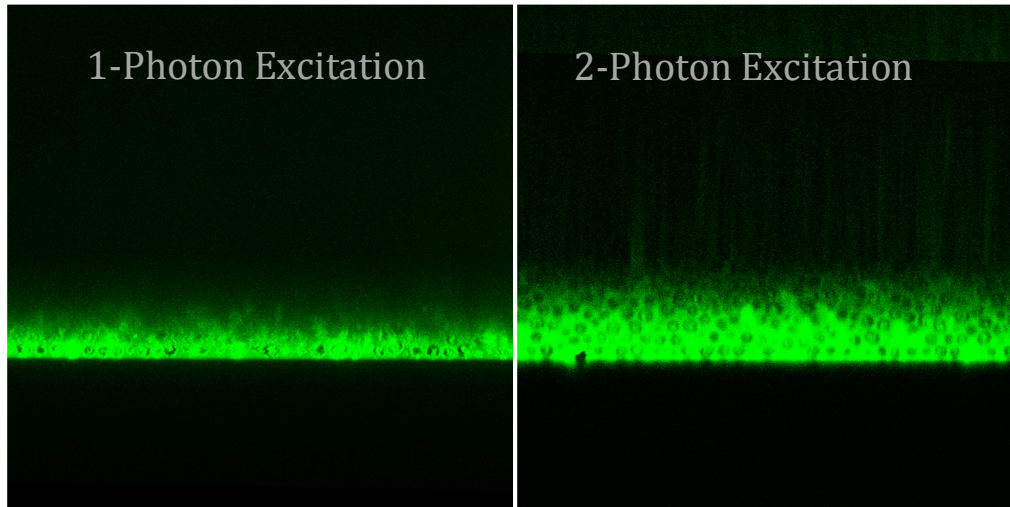
Figure 8. *XZ* scan of the yeast microcolony at the inverted microscope stand Leica DMIRE2 with SP2 confocal microscope. Left: conventional (1-photon excitation) scan; Right: scan of the same microcolony made with infrared pulsed laser Chameleon Ultra (Coherent Inc., California) for two-photon excitation (2PE) with excitation wavelength 920 nm. Due to longer wavelengths used for 2PE, it allows for deeper visualization into the yeast microcolony.

The finding that 2PE confocal microscopy provides much more information on colony structure when observing it either from the bottom or from the side into the structure also indicates an interesting possibility of using similar method for investigation of other microbial multicellular communities including natural biofilms. So our new approaches could also contribute to new insights on these structures and to the reconstruction of spatio-temporal changes in the presence of particular proteins connected with cell differentiation as well as other changes, which can reveal specificities of cells located at particular positions within microbial multicellular structures.

To conclude, new approach to the analysis of the intact (whole) yeast microcolonies was developed. The 2PE approach allowed revealing architecture of microcolonies. Also, this non-invasive technique enabled studies of the expression and spatio-temporal distribution of selected proteins (tagged with fluorescent markers or stained with specific dyes) in natural conditions.

Personal contribution:

In this project I have largely contributed to development and optimization of the 2PE microscopy approach to this particular biological object. I was responsible for the image acquisition, image processing and analysis.

Flo11p, drug efflux pumps, and the extracellular matrix cooperate to form biofilm yeast colonies

Libuše Váchová, Vratislav Šťovíček, Otakar Hlaváček, Oleksandr Chernyavskiy, Luděk Štěpánek, Lucie Kubínová, Zdena Palková, Journal of Cell Biology **194** (5) (2011), 679–687.

Much like other microorganisms, wild yeasts preferentially form surface-associated communities, such as biofilms and colonies, that are well protected against hostile environments and, when growing as pathogens, against the host immune system. However, the molecular mechanisms underlying the spatiotemporal development and environmental resistance of biofilms and colonies remain largely unknown.

The developmental principles, revealed in this study, provide new insights into the differentiation of a biofilm colony and the function of specialized cell subpopulations, and they suggest the presence of unique mechanisms of population protection. What are the colony strategies? A colony arising from a single cell grows very quickly, as most cells efficiently divide. In contrast to a smooth laboratory strain colony, biofilm colony also expands substantially in the vertical direction. This expansion may be enabled by the velcrolike interconnection of its cells. Initially, the colony population protects itself from external chemical threats by inducing MDR exporters (Fig. S2), capable of removing toxic compounds [159]. Later, the activity of the exporters persists exclusively in the surface cell layers over the entire colony, and, in parallel, additional protection strategies are initiated. The upper cell layers of the aerial part of the colony become stationary and thus more resistant to chemical and other threats. As the nutrients from agar are efficiently transported, the formation of such nondividing cells appears to be not simply the result of nutrient exhaustion but, more likely, a regulated process that helps to protect the colony surface that is directly exposed to the open air. In parallel, the internal cells near the agar begin to produce the ECM. The preservation of the velcrolike joints then contributes to the mechanical stability of the expanding colony and may lend flexibility to the layer, forming aerial wrinkles with internal cavities. Subsequent cell generations formed by the dividing inner cells of that layer are thus well protected. The cells in the inner bottom part of the ridge and the pseudohyphae in the subsurface colony regions do not enter a stationary phase. Rather, they continue to produce the ECM that is

impermeable to some small compounds such as galactose and to harmful chemicals such as copper ions. Only the pseudohyphae tips protrude from the ECM, but these are still protected by the MDR exporters. The tips may function as the sensors of nutrients and other environmental stimuli important to the colony. The questions remain as to what the chemical nature of the ECM is and how the embedded cells access the nutrients that are essential for their growth. It was previously shown that the ECMs of various microorganisms function as sorptive sponges that sequester organic molecules close to the cells [160] and that they also bind and sequester drugs [161]. Yeast ECMs vary by their content of different polymeric and monomeric carbohydrates, proteins, and phosphorus [162] and are even preferentially grazed by ciliates [163], suggesting that ECMs have nutritional value. Thus, we hypothesize that in the biofilm colony, the ECM itself may function both as a sequestration barrier and a nutrient pool essential for new cell progeny within the cavities.

In conclusion, the dynamics of the yeast microcolonies development was studied by means of 2PE confocal microscopy in combination with fluorescent protein tagging and staining methods. We revealed specific architecture of the biofilm colony that enables multiple protection strategies, yielding a high level of resistance in the wild. Importantly, some of the colony features that we have shown here (e.g., a specific growth pattern, the production of the ECM, and drug efflux pumps) are the traits that are also implicated in the formation of complex fungal biofilms [164]. Thus, the structured yeast colony represents a well-defined and powerful in vivo model system that may help to uncover the underlying general principles of microbial biofilm formation.

Personal contribution:

In this project I have largely contributed to development and optimization of the 2PE microscopy approach to this particular biological object. I was responsible for the image acquisition, image processing and analysis.

Imaging of mouse experimental melanoma in vivo and ex vivo by combination of confocal and nonlinear microscopy

Oleksandr Chernyavskiy, Luca Vannucci, Paolo Bianchini, Francesco Difato, Mustafa Saieh, Lucie Kubínová:, Microscopy Research and Technique **72** (6) (2009), 411–423.

In order to obtain sufficiently informative images of unstained tumor tissues and their modifications after hyperthermia treatment (HT), we investigated possibilities of the combination of the one- and two-photon excitation microscopy (1PE and 2PE accordingly) for examination of the experimental melanoma tissue *in vivo*, in mice under general anesthesia, and *ex vivo* on freshly harvested specimens. The mouse experimental melanoma structure was studied and compared with normal tissue from the same animal by using confocal and nonlinear microscopy techniques based on (i) one-photon excitation (1PE) fluorescence, (ii) 1PE reflectance, (iii) second harmonic generation (SHG) imaging, and (iv) two-photon excitation (2PE) autofluorescence.

In the present study, the various imaging modes brought different and often complementary information on the histology of tissues under study. The special emphasis has been made to visualizing unstained specimens, by 1PE (one-photon excited fluorescence and reflectance) and 2PE (including SHG imaging and two-photon excited autofluorescence).

The 1PE reflectance mode proved to be well applicable to unstained fresh tissues, allowing clear visualization of different layers both in the control skin flap and in the melanoma capsule (Figs. 3 and 5) up to the depth of 70 μm from the specimen surface using the intensity compensation due to light attenuation with depth, both by post-processing [152] or during the z-stack image acquisition. We were able to find valuable differences after the HT administration in comparison with untreated tissues by this technique, which provided us with images suitable for quantitative analysis of tumor morphology, as demonstrated in Table **1**.

Table 1. Maximum Euler-Poincaré characteristic (χ_{max}) measured in the images acquired in 1PE reflectance mode, using the excitation wavelength of 488 nm, from tumor tissue of the experimental melanomas, excised before HT treatment, 30 min after HT treatment, and 5 h after HT treatment. Measured values for six images per group, their mean, and standard deviation (SD) are shown. The data were evaluated by one-way ANOVA and Newman-Keuls post hoc test. There were found significant differences between all pairs of groups at 5% significance level.

Image number	χ_{max} (before HT treatment)	χ_{max} (30 min after HT treatment)	χ_{max} (5 hours after HT treatment)
1	1586	890	650
2	1131	672	474
3	1227	527	715
4	1151	885	790
5	1072	1239	315
6	1128	664	321
Mean	1216	813	544
SD	188	252	204

The changes in structure of mouse subcutaneous melanoma after microwave-induced HT were evaluated. The analysis was based on images acquired from fresh tissue of the experimental melanomas in 1PE reflectance mode, using the excitation wavelength of 488 nm. Tumors were obtained from untreated control mice or at a scheduled time after the HT treatment (either 30 minutes or 5 hours after HT). First, we preprocessed the grayscale images. The images were smoothed by Gaussian filter with standard deviation $\sigma = 1.5$ μm to decrease the level of noise in the images, and the image background was removed using a top-hat Lipschitz filter [165]. For evaluation of the "granularity" (cell aggregation in the tissue) of melanoma tissue, we measured the maximum Euler-Poincaré characteristic (χ_{max}). For this purpose, the Euler-Poincaré characteristic (i.e., the connectivity number [166]) of binary images obtained by thresholding of the grayscale image was calculated for thresholds ranging from 0 to 255 and the maximum value, determining χ_{max}, was found. This parameter was suitable for analysis of melanoma morphological

structure, reflecting e.g. clamping of cells, when larger aggregates were formed, leading to a decrease in χ_{max}.

Thus, we checked different spectral conditions and other settings of image acquisition, as well as combinations of the above imaging modalities, to fully exploit the potential of these techniques in the evaluation of treated and untreated cancer tissue morphology. We were able to find significant differences after the HT administration in comparison with untreated tissues by this technique, which provided us with images suitable for quantitative analysis of tumor morphology, as demonstrated in Table 1. The SHG imaging microscopy proved to be very suitable for detecting collagen fibers in our fresh tissue samples without any staining, considering the high specificity of SHG imaging microscopy for detection of fibrillar collagen (i.e., collagen type I), as demonstrated by several authors [113], [136], [140]. We believe such approach has a significant potential for non-invasive *in vivo* imaging both for experimental models on animals and humans.

In conclusion, for imaging cancer structures (both ex vivo and in vivo), we have used the combination of the 1PE and 2PE microscopy, offered by simultaneous application of confocal and nonlinear optical microscopy techniques in several acquisition modes. We have shown that such complex approach increased the level of information on the microscopic structures, facilitated the examination of interrelationships between functional and morphological aspects based on measurable optical properties of the tissues. Moreover, it enabled study of the collagen fiber network in relation to other tissues, and to identify invasive tumor cells, thus enhancing the diagnostic possibilities. Such approach was applied for *in vivo* examination of experimental melanoma for the first time and it is promising for translational studies in human.

Personal contribution:

In this project I have developed and optimized the 2PE microscopy approach to in vivo image acquisition on anesthetized animals and fixed sections. I was responsible for the image acquisition, image processing and analysis.

Visualization of Reinke's crystals in normal and cryptorchid testis

Viviana Kozina, David Geist, Lucie Kubínová, Ernest Bilić Hans Peter Karnthaler, Thomas Waitz, Jiří Janáček, Oleksandr Chernyavskiy, Ivan Krhen, Davor Ježek, Histochemistry and Cell Biology **135** (2) (2011), 215–228.

Discovered and described by Reinke [167], these crystals are found only in men with active spermatogenesis and testosterone production. Apart from the fact that Reinke's crystals are normal constituents of human Leydig cells, their nature and function are poorly understood.

The aim of our study was to investigate the properties of Reinke's crystals in men with the normal morphology of the testis (control group) and infertile patients diagnosed with cryptorchidism. 20 biopsies from infertile patients and six biopsies from men with regular spermatogenesis (20-30 years.) were used.

Reinke's crystals could be very helpful in the diagnosis of Leydig cell tumors since the presence of crystals is pathognomonic for the identification of such neoplasms [168], [169], [170], [171], [172].

A three dimensional (3D) reconstruction of Reinke's crystal was based on a series of confocal microscopic images, which were deconvolved in the Huygens Professional software package (Scientific Volume Imaging, Hilversum, Netherlands) by 'quick maximum likelihood estimation' (QMLE) algorithm using the experimental PSF. Subsequently, by means of Ellipse software environment, 3D images were smoothed by a Gaussian filter and segmented by thresholding of the image connected with manual corrections as necessary. Finally, triangulated isosurfaces of segmented crystals were generated and surface rendering was applied.

Reinke's crystals stained with H&E were easily recognized by confocal microscopy, since eosin induced fluorescence of crystals. Routine H&E slides of 7 μm thickness proved to be satisfactory. Confocal microscopy recorded various appearances of the crystals: some were small, having the size of 0.2-1 μm; other larger ones reached, as already stated, several micrometers. Some were exceptionally large, bearing 10–12 μm. While bright field microscopy failed to provide precise data on the edges of the crystal sections, confocal images detected their

polygonal shape and edges parallel to each other. Moreover, after applying deconvolution techniques to increase the resolution of confocal images [151], the polygonal shape of the crystal sections became much sharper and resembled that recorded by TEM. Based on the stacks of images, a 3D reconstruction of crystals could be made.

In general, there was no difference in appearance and other morphological features of crystals between control and cryptorchid specimens, apart from the frequency of the crystals which were more abundant in biopsies of patients with cryptorchidism.

In conclusion, we analyzed Reinke's crystals in specimens of the normal and cryptorchid testis by means of bright field, confocal and TEM and stereology. All aforesaid microscopy methods were useful in the visualization of the crystal. The stereological analysis established the increase in the number of Reinke's crystals in cryptorchid specimens. Section thickness of 70–300 nm proved to be optimal for crystallographic analysis of biocrystals.

Confocal microscopy proved to be very useful in the assessment of the shape and 3D reconstruction of the crystal. TEM analysis confirmed a hexagonal form of the crystal, while crystallographic data on sections of 70-300 nm thickness provided a better insight into the organization of the crystal lattice. Stereological analysis revealed a significant increase in the number of crystals in cryptorchid testes when compared with controls. Increased number of crystals in cryptorchid specimens leads to the assumption that the prolonged exposure to higher (abdominal) temperature might stimulate enzymes involved in the synthesis of the proteins of the crystal. However, the exact molecular nature of the crystal lattice remains in both normal and cryptorchid testis obscure. The 3D reconstructions of crystals have shown that a large crystal is sometimes accompanied by a number of smaller ones. Microscopy methods were useful in the visualization of the crystal.

In conclusion, the properties of Reinke's crystals (in man with the normal morphology of the testis (control group) and infertile patients diagnosed with cryptorchidism) were investigated also by confocal microscopy. On the basis of confocal images z-series (that underwent a complex image processing), a 3D reconstruction of crystals was possible. CLSM helped in identifying

the morphological features of the crystals, especially their shape and arrangement within the Leydig cell. The crystal's mutual 3D orientation was defined after image processing, improving the resolution of confocal images. Thus, the confocal microscopy approach with subsequent image processing by deconvolution and visualization of deconvolved images can fill the gap between TEM and conventional optical microscopy with image postprocessing.

Personal contribution:

In this project I have performed the confocal image acquisition, image deconvolution and analysis.

Conclusions

In conclusion, specific 2PE image acquisition techniques were developed and applied for studies of specific biologic samples. Earlier impossible investigations were performed for the first time. Quantitative improvements are transformed into qualitative discoveries. We tested our optimized procedures in the following biological studies, in cooperation with our colleagues from the Institute of Microbiology CAS, Faculty of Sciences, Charles University in Prague, and University of Zagreb (Croatia):

1) we developed new approach to the analysis of the whole intact yeast microcolonies in order to reveal it's architecture and to implement a non-invasive technique to follow the expression and spatio-temporal distribution of selected proteins (tagged with fluorescent markers or stained with specific dyes), in conditions close to natural ones;

2) we investigated possibilities of the combination of the 1PE and 2PE microscopy techniques for *in vivo* and *ex vivo* imaging of the experimental melanoma tissue in the mouse;

3) we investigated the properties of Reinke's crystals by confocal microscopy in men with the normal morphology of the testis (control group) and infertile patients diagnosed with cryptorchidism.

Improved image acquisition approaches described in present work can be applied for different biological problems, such as studies of intact biofilms or *in vivo* assessment of skin tumors, including possible clinical applications.

References

[1] E. K. Abbe, "Beiträge zur Theorie des Mikroskops und der mikroskopischen Wahrnehmung," *Archiv für Mikroskopische Anatomie,* vol. 9, no. 1, p. 413, 1873.

[2] E. Abbe, "A Contribution to the Theory of the Microscope and the nature of Microscopic Vision," *Proceedings of the Bristol Naturalists' Society,* vol. 1, p. 200–261, 1875.

[3] E. K. Abbe, "Note on the proper definition of the amplifying power of a lens or a lens-system," *J.Royal Microsc. Soc.,* vol. 4, pp. 348-351, 1884.

[4] F. R. Rayleigh Lord, "XXXI. Investigations in optics, with special reference to the spectroscope," *Philosophical Magazine Series 5,* vol. 8, no. 49, 1879.

[5] R. D. Allen, N. S. Allen and J. L. Travis, "Videoenhanced contrast, differential interference contrast (AVEC-DIC) microscopy: a new method capable of analyzing microtubule-related motility in the reticulopodial network of Allogromia laticollaris," *Cell Motil. Cytoskel.,* vol. 1, p. 291–302, 1981.

[6] S. Inoué, "Video image processing greatly enhances contrast, quality, and speed in polarization-based microscopy," *J. Cell Biol.,* vol. 89, p. 346–356, 1981.

[7] S. Inoué, Video microscopy, New York: Plenum Press, 1986.

[8] N. Callamaras and I. Parker, "Construction of a confocal microscope for real-time x-y and x-z imaging," *Cell Calcium,* vol. 26, no. 6, pp. 271-280, Dec 1999.

[9] M. G. L. Gustafsson, "Surpassing the lateral resolution limit by a factor of two using structured illumination microscopy," *Journal of Microscopy,* vol. 198, pp. 82-87, 2000.

[10] M. G. Gustafsson, L. Shao, P. M. Carlton, C. J. Wang, I. N. Golubovskaya, W. Z. Cande, D. A. Agard and J. W. Sedat, "Three-dimensional resolution doubling in wide-field fluorescence microscopy by structured illumination," *Biophysical Journal,* vol. 94, pp. 4957-4970, 2008.

[11] R. Heintzmann and C. Cremer, "Laterally modulated excitation microscopy: Improvements of resolution by using a diffraction grating," *Proceedings of SPIE,* vol. 3568, pp. 185-196, 1999.

[12] R. Heintzmann and G. Ficz, "Breaking the resolution limit in light microscopy," *Brief Funct Genomic Proteomic.,* vol. 5, no. 4, pp. 289-301, Dec 2006.

[13] C. Cremer, M. Hausmann, J. Bradl and B. Schneider, "Wave field microscope with detection point spread function". US patent 7,342,717, filed 10 July 1997 Patent 7,342,717, 10 July 1997.

[14] S. W. Hell and J. Wichmann, "Breaking the diffraction resolution limit by stimulated emission: stimulated-emission-depletion fluorescence microscopy," *Optics Letters,* vol. 19, no. 11, pp.

780-782, 1994.

[15] E. Betzig, G. H. Patterson, R. Sougrat, O. W. Lindwasser, S. Olenych, J. S. Bonifacino, M. W. Davidson, J. Lippincott-Schwartz and H. F. Hess, "Imaging intracellular fluorescent proteins at nanometer resolution," *Science,* vol. 313, no. 5793, pp. 1642-1645, 15 Sep 2006.

[16] R. E. Thompson, D. R. Larson and W. W. Webb, "Precise nanometer localization analysis for individual fluorescent probes," *Biophys J.,* vol. 82, no. 5, pp. 2775-2783, May 2002.

[17] M. J. Rust, M. Bates and X. Zhuang, "Sub-diffraction-limit imaging by stochastic optical reconstruction microscopy (STORM)," *Nat Methods.,* vol. 3, no. 10, pp. 793-795, Oct 2006.

[18] B. Shmaefsky, Biotechnology 101, Greenwood, 2006, p. 171.

[19] M. W. Davidson, "Janssen's Microscope," 1999. [Online]. Available: http://micro.magnet.fsu.edu/primer/museum/janssen.html. [Accessed 15 March 2015].

[20] F. Stelluti, Persio tradotto in verso sciolto e dichiarato, 1st edition ed., Rome: Giacomo Mascardi, 1630.

[21] R. Hooke, "Micrographia, or some physiological descriptions of minute bodies made by magnifying glasses with observations andinquiries thereupon," London, 1665.

[22] R. Hooke, "Microscopium, or, Some new discoveries made with and concerning microscopes," London, 1677.

[23] A. Van Leeuwenhoek, The Selected Works of Antony van Leeuwenhoek Containing His Microscopical Discoveries in Many of the Works of Nature, Arno Press, (Arno Press, 1977).

[24] O. Heimstädt, "Das Fluoreszenzmikroskop," *Z. Wiss. Mikrosk.,* vol. 28, p. 330–337, 1911.

[25] P. Ellinger and A. Hirt, "Mikroskopische Beobachtungen an lebenden Organen mit Demonstrationen (Intravitalmikroskopie)," *Arch. Exp. Pathol. Phar.,* vol. 147, p. 63, 1929.

[26] A. H. Coons, H. J. Creech and R. N. Jones, "Immunological properties of an antibody containing a fluorescent group," *Proc. Soc. Expt. Biol. Med.,* vol. 47, p. 200–202, 1941.

[27] A. H. Coons, H. J. Creech, R. N. Jones and E. Berliner, "The demonstration of pneumococcal antigen in tissues by the use of fluorescent antibody," *J. Immunol.,* vol. 45, p. 159–170, 1942.

[28] M. Chalfie, Y. Tu, G. Euskirchen, W. W. Ward and D. C. Prasher, "Green fluorescent protein as a marker for gene expression," *Science,* vol. 263, p. 802–805, 1994.

[29] F. Zernike, "Das Phasenkontrastverfahren bei der mikroskopischen Beobachtung," *Z. technische Physik,* vol. 16, p. 454–457, 1935.

[30] F. Zernike, "Phase contrast, a new method for the microscopic observation of transparent

objects," *Physica,* vol. 9, p. 974–986, 1942.

[31]   F. H. Smith, "Microscopic interferometry," *Research,* vol. 8, p. 385–395, 1955.

[32]   G. Nomarski, "Microinterféromètre différentiel à ondes polarisées," *J. Phys. Radium,* vol. 16, p. 9S–11S, 1955.

[33]   R. D. Allen, G. B. David and G. Nomarski, "The Zeiss-Nomarski differential interference equipment for transmitted-light microscopy," *Z. Wiss. Mikrosk.,* vol. 69, p. 193–221, 1969.

[34]   D. Axelrod, "Cell-substrate contacts illuminated by total internal reflection fluorescence," *J. Cell Biol.,* vol. 89, p. 141–145, 1981.

[35]   T. Funatsu, Y. Harada, M. Tokunaga, K. Saito and T. Yanagida, "Imaging of single fluorescent molecules and individual ATP turnovers by single myosin molecules in aqueous solution," *Nature,* vol. 374, p. 555–559, 1995.

[36]   D. Zenisek, J. A. Steyer and W. Almers, "Transport, capture and exocytosis of single synaptic vesicles at active zones," *Nature,* vol. 406, p. 849–854, 2000.

[37]   J. Schmoranzer, M. Goulian, D. Axelrod and S. M. Simon, "Imaging constitutive exocytosis with total internal reflection fluorescence microscopy," *J. Cell Biol.,* vol. 149, p. 23–32, 2000.

[38]   Koana, *Journal of the Illumination Engineering Institute,* vol. 26, no. 8, pp. 371-385, 1942.

[39]   M. Minsky.Patent 3013467, 1961.

[40]   M. D. Egger and M. Petráň, "New reflected-light microscope for viewing unstained brain and ganglion cells," *Science,* vol. 157, p. 305–307, 1967.

[41]   M. Minsky, "Memoir on inventing the confocal microscope," *Scanning,* vol. 10, p. 128–138, 1988.

[42]   C. J. Sheppard and T. Wilson, "The theory of the direct-view confocal microscope," *J. Microsc.,* vol. 124, p. 107–117, 1981.

[43]   J. G. White, W. B. Amos and M. Fordham, "The theory of the direct-view confocal microscope," *J. Microsc.,* vol. 124, p. 107–117, 1981.

[44]   J. G. White, W. B. Amos and M. Fordham, "An evaluation of confocal versus conventional imaging of biological structures by fluorescence light microscopy," *J. Cell Biol.,* vol. 105, p. 41–48, 1987.

[45]   G. Van Meer, E. H. K. Stelzer, R. W. Wijnaendts-van Resandt and K. Simons, "Sorting of sphingolipids in epithelial (Madin–Darby canine kidney) cells," *J. Cell Biol.,* vol. 105, p. 1623–1635, 1987.

[46] W. B. Amos and J. G. White, "How the confocal laser scanning microscope entered biological research," *Biol Cell.,* vol. 95, no. 6, pp. 335-342, Sep 2003.

[47] W. Denk, J. H. Strickler and W. W. Webb, "Two-photon laser scanning fluorescence microscopy," *Science,* vol. 248, no. 4951, pp. 73-76, 6 Apr 1990.

[48] G. J. Brakenhoff, J. Squier, T. Norris, A. C. Bliton, M. H. Wade and B. Athey, "Real-time two-photon confocal microscopy using a femtosecond, amplified Ti:sapphire system," *J Microsc.,* vol. 181, no. Pt 3, pp. 253-259, Mar 1996.

[49] C. Cremer and T. Cremer, "Considerations on a laser-scanning-microscope with high resolution and depth of field," *Microscopica Acta,* vol. 81, no. 1, pp. 31-44, 1978.

[50] C. J. Sheppard and R. Kompfner, "Resonant scanning optical microscope," *Applied Optics,* vol. 17, p. 2879–2882, 1978.

[51] T. Wilson and A. R. Carlini, "Three dimensional imaging in confocal imaging systems with finite-sized detectors," *J. Microsc.,* vol. 141, no. 1, pp. 51-66, 1988.

[52] G. J. Brakenhoff, "Imaging modes in confocal scanning light microscopy (CSLM)," *J. Microsc.,* vol. 117, pp. 233-242, 1979.

[53] G. J. Brakenhoff, P. Blom and P. Barends, "Confocal scanning light microscopy with high aperture immersion lenses," *Journal of Microscopy,* pp. 219-232, November 1979.

[54] K. Carlsson, P. E. Danielsson, R. Lenz, A. Liljeborg, L. Majlöf and N. Åslund, "Three-dimensional microscopy using a confocal laser scanning microscope," *Optics Letters,* vol. 10, no. 2, pp. 53-55, 1985.

[55] K. Carlsson and N. Åslund, *Applied Optics,* vol. 26, no. 16, pp. 3232-3238, 15 August 1987.

[56] M. Petráň, M. Hadravský, M. D. Egger and R. Galambos, "Tandem-Scanning Reflected-Light Microscope," *J. Opt. Soc. Am.,* vol. 58, no. 5, pp. 661-664, 1968.

[57] S. Johnson, "Light Microscopy Core Facility, Duke University and Duke University Medical Center," 2015. [Online]. Available: http://microscopy.duke.edu/learn/introtomicroscopy/twophotonex.html. [Accessed 20 Mar 2015].

[58] M. Rajadhyaksha, M. Grossman, D. Esterowitz and R. H. Webb, "In vivo confocal scanning laser microscopy of human skin: melanin provides strong contrast," *J Invest Dermatol.,* vol. 104, no. 6, pp. 946-952, Jun 1995.

[59] M. Rajadhyaksha, S. González, J. M. Zavislan, R. R. Anderson and R. H. Webb, "In vivo confocal scanning laser microscopy of human skin II: advances in instrumentation and comparison with histology," *J Invest Dermatol.,* vol. 113, no. 3, pp. 293-303, Sep 1999.

[60] S. González, M. Rajadhyaksha and R. R. Anderson, "Non-invasive (real-time) imaging of histologic margin of a proliferative skin lesion in vivo," *J Invest Dermatol.,* vol. 111, no. 3, pp. 538-539, Sep 1998.

[61] S. González, E. González, W. M. White and M. Rajadhyaksha, "Allergic contact dermatitis: correlation of in vivo confocal imaging to routine histology," *J Am Acad Dermatol.,* vol. 40, no. 5 Pt 1, pp. 708-713, May 1999.

[62] L. Hoogedoorn, M. Peppelman, P. C. van de Kerkhof, P. E. van Erp and M. J. Gerritsen, "The value of in vivo Reflectance Confocal Microscopy in monitoring and diagnosis of inflammatory and infectious skin diseases - A Systematic Review," *Br J Dermatol.,* 30 Oct 2014.

[63] K. Sokolov, K. B. Sung, T. Collier, A. Clark, D. Arifler, A. Lacy, M. Descour and R. Richards-Kortum, "Endoscopic microscopy," *Dis Markers.,* vol. 18, no. 5-6, pp. 269-291, 2002.

[64] J. Tan, P. Delaney and W. J. McLaren, "Confocal endomicroscopy: a novel imaging technique for in vivo histology of cervical intraepithelial neoplasia," *Expert Rev Med Devices.,* vol. 4, no. 6, pp. 863-871, Nov 2007.

[65] L. Mastropasqua, L. Agnifili, R. Mastropasqua, V. Fasanella, M. Nubile, L. Toto, P. Carpineto and M. Ciancaglini, "In vivo laser scanning confocal microscopy of the ocular surface in glaucoma," *Microsc Microanal.,* vol. 20, no. 3, pp. 879-894, Jun 2014.

[66] I. Jalbert, F. Stapleton, E. Papas, D. F. Sweeney and M. Coroneo, "In vivo confocal microscopy of the human cornea," *Br J Ophthalmol.,* vol. 87, no. 2, pp. 225-236, Feb 2003.

[67] A. Einstein, "On a Heuristic Point of View Concerning the Production and Transformation of Light," *Annalen der Physik,* vol. 17, p. 132–148, 1905.

[68] M. Göppert-Mayer, "Über Elementarakte mit zwei Quantensprüngen," *Annals of Physics,* vol. 9, no. 3, p. 273–295, 1931.

[69] A. Diaspro, G. Chirico and M. Collini, "Two-photon fluorescence excitation and related techniques in biological microscopy," *Q Rev Biophys.,* vol. 38, no. 2, pp. 97-166, May 2005.

[70] W. Kaiser and C. G. Garrett, "Two-photon excitation in $CaF_2:Eu^{2+}$," *Physical Review Letters,* vol. 7, no. 6, p. 229–232, 1961.

[71] W. Denk and K. Svoboda, "Photon upmanship: why multiphoton imaging is more than a gimmick," *Neuron,* vol. 18, no. 3, pp. 351-357, Mar 1997.

[72] M. Oheim, D. J. Michael, M. Geisbauer, D. Madsen and R. H. Chow , "Principles of two-photon excitation fluorescence microscopy and other nonlinear imaging approaches," *Adv Drug Deliv Rev.,* vol. 58, no. 7, pp. 788-808, 15 Sep 2006.

[73] M. D. Cahalan, I. Parker, S. H. Wei and M. J. Miller, "Two-photon tissue imaging: seeing the

immune system in a fresh light," *Nat Rev Immunol.,* vol. 2, no. 11, pp. 872-880, Nov 2002.

[74] W. A. Mohler, J. S. Simske, E. M. Williams-Masson, J. D. Hardin and J. G. White, "Dynamics and ultrastructure of developmental cell fusions in the Caenorhabditis elegans hypodermis," *Curr Biol.,* vol. 8, no. 19, pp. 1087-1090, 24 Sep 1998.

[75] C. W. Randall, "Examining live embryos nondestructively," *Biophotonics Int.,* pp. 42-44, Nov-Dec 1999.

[76] O. Nakamura, "Fundamental of two-photon microscopy," *Microsc Res Tech.,* vol. 47, no. 3, pp. 165-171, 1 Nov 1999.

[77] W. Denk, D. W. Piston and W. W. Webb, "Two-photon molecular excitation in laser-scanning microscopy," in *Handbook of Biological Confocal Microscopy*, J. B. Pawley, Ed., New York, Plenum Press, 1995, p. 445–458.

[78] G. H. Patterson and D. W. Piston, "Photobleaching in two-photon excitation microscopy," *Biophys J.,* vol. 78, no. 4, pp. 2159-2162, Apr 2000.

[79] P. J. Campagnola and L. M. Loew, "Second-harmonic imaging microscopy for visualizing biomolecular arrays in cells, tissues and organisms," *Nat Biotechnol.,* vol. 21, no. 11, pp. 1356-1360, Nov 2003.

[80] W. R. Zipfel, R. M. Williams and W. W. Webb, "Nonlinear magic: multiphoton microscopy in the biosciences," *Nat Biotechnol.,* vol. 21, no. 11, pp. 1369-1377, Nov 2003.

[81] F. Cella and A. Diaspro, "Two-photon excitation microscopy: a superb wizard for fluorescence imaging," in *Nanoscopy and Multidimensional Optical Fluorescence Microscopy*, A. Diaspro, Ed., Boca Raton London New York, Taylor & Francis Group, 2010, pp. 7-1 - 7-12.

[82] A. Diaspro, M. Corosu, P. Ramoino and M. Robello, "Adapting a compact confocal microscope system to a two-photon excitation fluorescence imaging architecture," *Microsc Res Tech.,* vol. 47, no. 3, pp. 196-205, 1 Nov 1999.

[83] X. Chen, O. Nadiarynkh, S. Plotnikov and P. J. Campagnola, "Second harmonic generation microscopy for quantitative analysis of collagen fibrillar structure," *Nat Protoc.,* vol. 7, no. 4, pp. 654-669, 8 Mar 2012.

[84] H. C. Gerritsen and C. J. De Grauw, "Imaging of optically thick specimen using two-photon excitation microscopy," *Microsc Res Tech.,* vol. 47, no. 3, pp. 206-209, 1 Nov 1999.

[85] C. Xu and W. W. Webb, "Measurement of two-photon excitation cross sections of molecular fluorophores with data from 690 to 1050 nm," *J.Opt.Soc.Am.B,* vol. 13, no. 3, pp. 481-491, 1996.

[86] F. Bestvater, E. Spiess, G. Stobrawa, M. Hacker, T. Feurer, T. Porwol, U. Berchner-Pfannschmidt, C. Wotzlaw and H. Acker, "Two-photon fluorescence absorption and emission spectra of dyes

relevant for cell imaging," *J Microsc.,* vol. 208, no. Pt 2, pp. 108-115, Nov 2002.

[87] K. G. Heinze, A. Koltermann and P. Schwille, "Simultaneous two-photon excitation of distinct labels for dual-color fluorescence crosscorrelation analysis," *PNAS,* vol. 97, no. 19, p. 10377–10382, 12 Sep 200.

[88] C. Xu, W. Zipfel, J. B. Shear, R. M. Williams and W. W. Webb, "Multiphoton fluorescence excitation: new spectral windows for biological nonlinear microscopy," *Proc Natl Acad Sci USA,* vol. 93, no. 20, pp. 10763-10768, 1 Oct 1996.

[89] Y. Zeng, B. Yan, Q. Sun, S. He, J. Jiang, Z. Wen and J. Y. Qu, "In vivo micro-vascular imaging and flow cytometry in zebrafish using two-photon excited endogenous fluorescence," *Biomed Opt Express.,* vol. 5, no. 3, pp. 653-663, 4 Feb 2014.

[90] A. T. Young, "Rayleigh scattering," *Appl. Opt.,* vol. 20, no. 4, p. 522–535, 15 Feb 1981.

[91] D. W. Piston, "When two is better than one: elements of intravital microscopy," *PLoS Biol.,* vol. 3, no. 6, p. e207, 14 Jun 2005.

[92] M. Schneider, S. Barozzi, I. Testa, M. Faretta and A. Diaspro, "Two-photon activation and excitation properties of PA-GFP in the 720-920-nm region," *Biophys J.,* vol. 89, no. 2, pp. 1346-1352, 20 May 2005.

[93] D. Mazza, F. Cella, G. Vicidomini, S. Krol and A. Diaspro, "Role of three-dimensional bleach distribution in confocal and two-photon fluorescence recovery after photobleaching experiments," *Appl Opt.,* vol. 46, no. 30, pp. 7401-7411, 20 Oct 2007.

[94] A. Ustione and D. W. Piston, "A simple introduction to multiphoton microscopy," *J Microsc.,* vol. 243, no. 3, pp. 221-226, Sep 2011.

[95] E. Beaurepaire, M. Oheim and J. Mertz, "Ultra-deep two-photon fluorescence excitation in turbid media," *Opt. Commun.,* vol. 188, no. 1-4, p. 25–29, 1 Feb 2001.

[96] P. Theer, M. T. Hasan and W. Denk, "Two-photon imaging to a depth of 1000 um in living brains by use of a Ti: Al2O3 regenerative amplifier," *Opt. Lett.,* vol. 28, p. 1022–1024, 2003.

[97] D. Kobat, M. E. Durst, N. Nishimura, A. W. Wong, C. B. Schaffer and C. Xu, "Deep tissue multiphoton microscopy using longer wavelength excitation," *Opt Express.,* vol. 17, no. 16, pp. 13354-13364, 3 Aug 2009.

[98] D. Kobat, N. G. Horton and C. Xu, "In vivo two-photon microscopy to 1.6-mm depth in mouse cortex," *J Biomed Opt.,* vol. 16, no. 10, p. 106014, Oct 2011.

[99] K. Svoboda and R. Yasuda, "Principles of Two-Photon Excitation Microscopy and Its Applications to Neuroscience," *Neuron,* vol. 50, no. 6, p. 823–839, 15 June 2006.

[100] W. Denk, K. R. Delaney, A. Gelperin, D. Kleinfeld, B. W. Strowbridge, D. W. Tank and R. Yuste, "Anatomical and functional imaging of neurons using 2-photon laser scanning microscopy," *J Neurosci Methods.,* vol. 54, no. 2, pp. 151-162, 1994.

[101] D. W. Piston, B. R. Masters and W. W. Webb, "Three-dimensionally resolved NAD(P)H cellular metabolic redox imaging of the in situ cornea with two-photon excitation laser scanning microscopy," *J Microsc.,* vol. 178, no. Pt 1, pp. 20-27, 1995.

[102] E. Yew, C. Rowlands and P. T. So, "Application of Multiphoton Microscopy in Dermatological Studies: a Mini-Review," *J Innov Opt Health Sci.,* vol. 7, no. 5, p. 1330010, 3 Jan 2014.

[103] K. König K, P. T. So, W. W. Mantulin, B. J. Tromberg and E. Gratton, "Two-photon excited lifetime imaging of autofluorescence in cells during UVA and NIR photostress," *J Microsc.,* vol. 183, no. Pt 3, pp. 197-204, Sep 1996.

[104] P. T. So, K. König, K. Berland, C. Y. Dong, T. French, C. Bühler, T. Ragan and E. Gratton, "New time-resolved techniques in two-photon microscopy," *Cell Mol Biol (Noisy-le-grand),* vol. 44, no. 5, pp. 771-793, Jul 1998.

[105] R. N. Germain, E. A. Robey and M. D. Cahalan, "A decade of imaging cellular motility and interaction dynamics in the immune system," *Science,* vol. 336, no. 6089, pp. 1676-1681, 29 Jun 2012.

[106] K. König, "Clinical multiphoton tomography," *Journal of Biophotonics,* vol. 1, no. 1, 14 Jan 2008.

[107] L. Moreaux, O. Sandre and J. Mertz, "Membrane imaging by second-harmonic generation microscopy," *J.Opt.Soc.Am.B,* vol. 17, no. 10, pp. 1685-1694, 2000.

[108] J. Mertz and L. Moreaux, "Second-harmonic generation by focused excitation of inhomogeneously distributed scatterers," *Optics Communications,* vol. 196, no. 1-6, p. 325–330, 1 Sep 2001.

[109] I. Freund, M. Deutsch and A. Sprecher, "Connective tissue polarity. Optical second-harmonic microscopy, crossed-beam summation, and small-angle scattering in rat-tail tendon," *Biophys J.,* vol. 50, no. 4, pp. 693-712, Oct 1986.

[110] P. J. Campagnola, A. C. Millard, M. Terasaki, P. E. Hoppe, C. J. Malone and W. A. Mohler, "Three-dimensional high-resolution second-harmonic generation imaging of endogenous structural proteins in biological tissues," *Biophys J.,* vol. 82, no. 1, pp. 493-508, Jan 2002.

[111] A. Erikson, J. Ortegren, T. Hompland, C. de Lange Davies and M. Lindgren, "Quantification of the second-order nonlinear susceptibility of collagen I using a laser scanning microscope," *J Biomed Opt.,* vol. 12, no. 4, p. 044002, Jul-Aug 2007.

[112] R. M. Williams, W. R. Zipfel and W. W. Webb, "Interpreting second-harmonic generation images of collagen I fibrils," *Biophys J.,* vol. 88, no. 2, pp. 1377-1386, Feb 2005.

[113] A. Zoumi, A. Yeh and B. J. Tromberg, "Imaging cells and extracellular matrix in vivo by using second-harmonic generation and two-photon excited fluorescence," *Proc Natl Acad Sci USA,* vol. 99, no. 17, pp. 11014-11019, 20 Aug 2002.

[114] P. Franken, A. Hill, C. Peters and G. Weinreich, "Generation of Optical Harmonics," *Physical Review Letters,* vol. 7, no. 4, pp. 118-119, 1961.

[115] Y. R. Shen, "Surface properties probed by second-harmonic and sum-frequency generation," *Nature,* vol. 337, 09 February 1989.

[116] R. Hellwarth and P. Christensen, "Nonlinear microscopic examination of structure in polycrystalline ZnSe," *Opt. Commun.,* vol. 12, p. 318–322, 1974.

[117] K. B. Eisenthal, "Liquid Interfaces Probed by Second-Harmonic and Sum-Frequency Spectroscopy," *Chem Rev.,* vol. 96, no. 4, pp. 1343-1360, 20 Jun 1996.

[118] C. J. Sheppard, R. Kompfner, J. Gannaway and D. Walsh, "The scanning harmonic optical microscope," *IEEE J. Quantum Electron.,* Vols. QE-13, p. 100D, 1977.

[119] J. Gannaway and C. J. Sheppard, "Second harmonic imaging in the scanning optical microscope," *Opt. and Quant. Elec.,* vol. 10, pp. 435-439, 1978.

[120] R. Gauderon R, P. B. Lukins and C. J. Sheppard, "Three-dimensional second-harmonic generation imaging with femtosecond laser pulses," *Opt Lett.,* vol. 23, no. 15, pp. 1209-1211, 1 Aug 1998.

[121] J. Y. Huang, A. Lewis and L. Loew, "Nonlinear optical properties of potential sensitive styryl dyes," *Biophys J.,* vol. 53, no. 5, pp. 665-670, May 1988.

[122] O. Bouevitch, A. Lewis, I. Pinevsky, J. P. Wuskell and L. M. Loew, "Probing membrane potential with nonlinear optics," vol. 65, no. 2, pp. 672-679, Aug 1993.

[123] I. Ben-Oren, G. Peleg, A. Lewis, B. Minke and L. Loew, "Infrared nonlinear optical measurements of membrane potential in photoreceptor cells," *Biophys J.,* vol. 71, no. 3, pp. 1616-1620, 1996.

[124] G. Peleg, A. Lewis, M. Linial and L. M. Loew, "Nonlinear optical measurement of membrane potential around single molecules at selected cellular sites," *Proc Natl Acad Sci USA,* vol. 96, no. 12, pp. 6700-6704, 8 Jun 1999.

[125] A. Lewis, A. Khatchatouriants, M. Treinin, Z. Chen, G. Peleg, N. Friedman, O. Bouevitch, Z. Rothman, L. Loew and M. Sheves, "Second harmonic generation of biological interfaces: Probing the membrane protein bacteriorhodopsin and imaging membrane potential around GFP molecules at specific sites in neuronal cells of C.elegans," *Chem. Phys.,* vol. 245, p. 133–144, 1999.

[126] P. J. Campagnola, M. D. Wei, A. Lewis and L. M. Loew, "High-resolution nonlinear optical imaging of live cells by second harmonic generation," *Biophys J.,* vol. 77, no. 6, pp. 3341-3349, Dec 1999.

[127] W. Mohler, A. C. Millard and P. J. Campagnola, "Second harmonic generation imaging of endogenous structural proteins," *Methods.,* vol. 29, no. 1, pp. 97-109, Jan 2003.

[128] A. Keikhosravi, J. S. Bredfeldt, A. K. Sagar and K. W. Eliceiri, "Second-harmonic generation imaging of cancer," *Methods Cell Biol.,* vol. 123, pp. 531-546, 2014.

[129] L. C. Chen, W. R. Lloyd, S. Kuo, H. M. Kim, C. L. Marcelo, S. E. Feinberg and M. A. Mycek, "The potential of label-free nonlinear optical molecular microscopy to non-invasively characterize the viability of engineered human tissue constructs," *Biomaterials.,* vol. 35, no. 25, pp. 6667-6676, Aug 2014.

[130] S. J. Matcher, "What can biophotonics tell us about the 3D microstructure of articular cartilage?," *Quant Imaging Med Surg.,* vol. 5, no. 1, pp. 143-158, Feb 2015.

[131] J. V. Jester, M. Winkler and B. E. Jester, *Eye Contact Lens.,* vol. 36, no. 5, pp. 260-264, Sep 2010.

[132] K. G. Brockbank, W. R. MacLellan, J. Xie, S. F. Hamm-Alvarez, Z. Z. Chen and K. Schenke-Layland, "Quantitative second harmonic generation imaging of cartilage damage," *Cell Tissue Bank,* vol. 9, no. 4, pp. 299-307, Dec 2008.

[133] G. Cox, E. Kable, A. Jones, I. Fraser, F. Manconi and M. D. Gorrell, "3-dimensional imaging of collagen using second harmonic generation," *J Struct Biol.,* vol. 141, no. 1, pp. 53-62, Jan 2003.

[134] J. C. Mansfield, C. P. Winlove, J. Moger and S. J. Matcher, "Collagen fiber arrangement in normal and diseased cartilage studied by polarization sensitive nonlinear microscopy," *J Biomed Opt.,* vol. 13, no. 4, p. 044020, Jul-Aug 2008.

[135] J. Chen, S. Zhuo, T. Luo, X. Jiang and J. Zhao, "Spectral characteristics of autofluorescence and second harmonic generation from ex vivo human skin induced by femtosecond laser and visible lasers," *Scanning,* vol. 28, no. 6, pp. 319-326, Nov-Dec 2006.

[136] E. Brown, T. McKee, E. diTomaso, A. Pluen, B. Seed, Y. Boucher and R. K. Jain, "Dynamic imaging of collagen and its modulation in tumors in vivo using second-harmonic generation," *Nat Med.,* vol. 9, no. 6, pp. 796-800, Jun 2003.

[137] A. M. Pena, A. Fabre, D. Débarre, J. Marchal-Somme, B. Crestani, J. L. Martin, E. Beaurepaire and M. C. Schanne-Klein, "Three-dimensional investigation and scoring of extracellular matrix remodeling during lung fibrosis using multiphoton microscopy," *Microsc Res Tech.,* vol. 70, no. 2, pp. 162-170, Feb 2007.

[138] P. P. Provenzano, K. W. Eliceiri, J. M. Campbell, D. R. Inman, J. G. White and P. J. Keely, "Collagen reorganization at the tumor-stromal interface facilitates local invasion," *BMC Med.,*

vol. 4, no. 1, p. 38, 26 Dec 2006.

[139] E. C. Rothstein, M. Nauman, S. Chesnick and R. S. Balaban, "Multi-photon excitation microscopy in intact animals," *J Microsc.,* vol. 222, no. Pt 1, pp. 58-64, Apr 2006.

[140] M. Strupler, A. M. Pena, M. Hernest, P. L. Tharaux, J. L. Martin, E. Beaurepaire and M. C. Schanne-Klein, "Second harmonic imaging and scoring of collagen in fibrotic tissues," *Opt Express.,* vol. 15, no. 7, pp. 4054-4065, 2 Apr 2007.

[141] A. Zoumi, X. Lu, G. S. Kassab and B. J. Tromberg, "Imaging coronary artery microstructure using second-harmonic and two-photon fluorescence microscopy," *Biophys J.,* vol. 87, no. 4, pp. 2778-2786, Oct 2004.

[142] W. L. Chen, Y. Sun, W. Lo, H. Y. Tan and C. Y. Dong, "Combination of multiphoton and reflective confocal imaging of cornea," *Microsc Res Tech.,* vol. 71, no. 2, pp. 83-85, Feb 2008.

[143] P. Anikijenko, L. T. Vo, E. R. Murr, J. Carrasco, W. J. McLaren, Q. Chen, S. G. Thomas, P. M. Delaney and R. G. King, "In vivo detection of small subsurface melanomas in athymic mice using noninvasive fiber optic confocal imaging," *J Invest Dermatol.,* vol. 117, no. 6, pp. 1442-1448, Dec 2001.

[144] Y. Li, S. Gonzalez, T. H. Terwey, J. Wolchok, Y. Li, I. Aranda, R. Toledo-Crow and A. C. Halpern, "Dual mode reflectance and fluorescence confocal laser scanning microscopy for in vivo imaging melanoma progression in murine skin," *J Invest Dermatol.,* vol. 125, no. 4, pp. 798-804, Oct 2005.

[145] A. Erikson, J. Ortegren, T. Hompland, C. de Lange Davies and M. Lindgren, "Quantification of the second-order nonlinear susceptibility of collagen I using a laser scanning microscope," *J Biomed Opt.,* vol. 12, no. 4, p. 044002, Jul-Aug 2007.

[146] P. Wust, B. Hildebrandt, G. Sreenivasa, B. Rau, J. Gellermann, H. Riess, R. Felix and P. M. Schlag, "Hyperthermia in combined treatment of cancer," *Lancet Oncol.,* vol. 3, no. 8, pp. 487-497, Aug 2002.

[147] P. J. Verveer, Computational and Optical Methods for Improving Resolution and Signal Quality in Fluorescence Microscopy, Göttingen: Delft University of Technology, 1998.

[148] M. Schrader, S. W. Hell and H. T. van der Voort, "Potential of confocal microscopes to resolve in the 50-100 nm range," *Appl. Phys. Lett.,* vol. 69, no. 24, pp. 3644-3646, 1996.

[149] H. Kano, H. T. van der Voort, M. Schrader, G. M. P. van Kempen and S. W. Hell, "Avalanche photodiode detection with object scanning and image restoration provides 2-4 fold resolution increase in two-photon fluorescence microscopy," *Bioimaging,* vol. 4, no. 3, pp. 187-197, 1996.

[150] V. Schoonderwoert, R. Dijkstra, G. Luckinavicius, O. Kobler and H. T. M. van der Voort, "Huygens STED Deconvolution Increases Signal-To-Noise And Image Resolution Towards 22

nm," vol. 21, no. 6, 2013.

[151] Y. Cotte, M. F. Toy, N. Pavillon and C. Depeursinge, "Microscopy image resolution improvement by deconvolution of complex fields," *Opt Express,* vol. 18, no. 19, pp. 19462-19478, 13 Sep 2010.

[152] M. Čapek, J. Janáček and L. Kubínová, "Methods for compensation of the light attenuation with depth of images captured by a confocal microscope," *Microsc Res Tech.,* vol. 69, no. 8, pp. 624-635, Aug 2006.

[153] L. Váchová, V. Stovícek, O. Hlavácek, O. Chernyavskiy, L. Stěpánek, L. Kubínová and Z. Palková, "Flo11p, drug efflux pumps, and the extracellular matrix cooperate to form biofilm yeast colonies," *J Cell Biol.,* vol. 194, no. 5, pp. 679-687, 5 Sep 2011.

[154] S. Preibisch, S. Saalfeld and P. Tomancak, "Globally optimal stitching of tiled 3D microscopic image acquisitions," *Bioinformatics,* vol. 25, no. 11, pp. 1463-1465, 1 Jun 2009.

[155] O. Chernyavskiy, L. Vannucci, P. Bianchini, F. Difato, M. Saieh and L. Kubínová, "Imaging of mouse experimental melanoma in vivo and ex vivo by combination of confocal and nonlinear microscopy," *Microsc Res Tech.,* vol. 72, no. 6, pp. 411-423, Jun 2009.

[156] J. Schindelin, I. Arganda-Carreras, E. Frise, V. Kaynig, M. Longair, T. Pietzsch, S. Preibisch, C. Rueden, S. Saalfeld, B. Schmid, J. Y. Tinevez, D. J. White, V. Hartenstein, K. Eliceiri, P. Tomancak and A. Cardona, "Fiji: an open-source platform for biological-image analysis," *Nat Methods,* vol. 9, no. 7, pp. 676-682, 28 Jun 2012.

[157] C. A. Schneider, W. S. Rasband and K. W. Eliceiri, "NIH Image to ImageJ: 25 years of image analysis," *Nat Methods,* vol. 9, no. 7, pp. 671-675, Jul 1997-2014.

[158] M. D. Abramoff, P. J. Magalhaes and S. J. Ram, "Image Processing with ImageJ," *Biophotonics International,* vol. 11, no. 7, pp. 36-42, 2004.

[159] G. Sipos and K. Kuchler, "Fungal ATP-binding cassette (ABC) transporters in drug resistance & detoxification," *Curr Drug Targets.,* vol. 7, no. 4, pp. 471-481, Apr 2006.

[160] A. W. Decho, "Microbial biofilms in intertidal systems: an overview," *Cont.Shelf Res.,* vol. 20, p. 1257–1273, 2000.

[161] J. E. Nett, H. Sanchez, M. T. Cain and D. R. Andes, "Genetic basis of Candida biofilm resistance due to drug-sequestering matrix glucan," *J Infect Dis.,* vol. 202, no. 1, p. 171–175, 1 Jul 2010.

[162] M. A. Al-Fattani and L. J. Douglas, "Biofilm matrix of Candida albicans and Candida tropicalis: chemical composition and role in drug resistance," *J Med Microbiol.,* vol. 55, no. Pt 8, pp. 999-1008, Aug 2006.

[163] L. M. Joubert, G. M. Wolfaardt and A. Botha, "Microbial exopolymers link predator and prey in

a model yeast biofilm system," *Microb Ecol.,* vol. 52, no. 2, pp. 187-97, Aug 2006.

[164] J. R. Blankenship and A. P. Mitchell, "How to build a biofilm: a fungal perspective," *Curr Opin Microbiol.,* vol. 9, no. 6, pp. 588-594, Dec 2006.

[165] M. Štencel and J. Janáček, "On calculation of chamfer distance and Lipschitz covers in digital images," in *Proceedings S4G*, Prague, 2006.

[166] J. Serra, Image analysis and mathematical morphology, London: Academic Press, 1982.

[167] F. Reinke, "Beiträge zur Histologie des Menschen. I. Űber Krystalloidbildungen in den interstitiellen Zellen des menschlichen Hodens," *Arch Mikr Anat.,* vol. 47, pp. 34-44, 1896.

[168] A. Assi, M. Sironi, A. M. Bacchioni, P. Declich, L. Cozzi and G. Pasquinelli, "Leydig cell tumor of the testis: a cytohistological, immunohistochemical, and ultrastructural case study," *Diagn Cytopathol.,* vol. 16, no. 3, pp. 262-266, Mar 1997.

[169] S. K. Gupta, I. M. Francis, Z. A. Sheikh, N. A. al-Rubah and D. K. Das, "Intranuclear Reinke's crystals in a testicular Leydig cell tumor diagnosed by aspiration cytology. A case report.," *Acta Cytol.,* pp. 252-256, Mar-Apr 1994.

[170] M. Jain, H. M. Aiyer, P. Bajaj and S. Dhar, "Intracytoplasmic and intranuclear Reinke's crystals in a testicular Leydig-cell tumor diagnosed by fine-needle aspiration cytology: a case report with review of the literature," *Diagn Cytopathol.,* vol. 25, no. 3, pp. 162-164, Sep 2001.

[171] F. Marino, G. Ferrara, G. Rapisarda and V. Galofaro, "Reinke's crystals in an interstitial cell tumour of a rabbit (Oryctolagus cuniculus)," *Reprod Domest Anim.,* vol. 38, no. 5, pp. 421-422, Oct 2003.

[172] M. M. Pérez, V. J. Puerta and M. Sánchez González, "An occult Leydig-cell tumor in a cryptorchid testis," *Arch Esp Urol.,* vol. 52, no. 1, pp. 76-78, Jan-Feb 1999.

List of figures

List of publications

(with IF of the journal for year of publication / partial IF / cumulative partial IF. Partial IF is calculated as *pIF* = Journal IF / (number of authors + 2), being 2·*pIF* for the first and last authors, and *pIF* for all other co-authors)

1. Oleksandr Chernyavskiy, Luca Vannucci, Paolo Bianchini, Francesco Difato, Mustafa Saieh, Lucie Kubínová, *Imaging of mouse experimental melanoma in vivo and ex vivo by combination of confocal and nonlinear microscopy*, Microscopy Research and Technique **72** (2009), pp. 411 – 423 (PMID: 19208388; IF: 1.85 / 0.4625 / 0.4625).

2. Libuše Váchová, Oleksandr Chernyavskiy, Dita Strachotová, Paolo Bianchini, Zuzana Burdíková, Ivana Ferčíková, Lucie Kubínová, Zdena Palková, *Architecture of developing multicellular yeast colony: spatio-temporal expression of Ato1p ammonium exporter*, Environmental Microbiology **11** (2009), pp. 1866 – 1877 (PMID: 19302539; IF: 4.909 / 0.4909 / 0.9534).

3. Viviana Kozina, David Geist, Lucie Kubínová, Ernest Bilić, Hans Peter Karnthaler, Thomas Waitz, Jiří Janáček, Oleksandr Chernyavskiy, Ivan Krhen, Davor Ježek, *Visualization of Reinke's crystals in normal and cryptorchid testis*, Histochemistry and Cell Biology, **135** (2011), pp. 215 – 228 (PMID: 21287192; IF: 2.588 / 0.2157 / 1.1691).

4. Libuše Váchová, Vratislav Šťovíček, Otakar Hlaváček, Oleksandr Chernyavskiy, Luděk Štěpánek, Lucie Kubínová, Zdena Palková, *Flo11p, drug efflux pumps, and the extracellular matrix cooperate to form biofilm yeast colonies*, Journal of Cell Biology **194** (2011), pp. 679 – 687 (PMID: 21875945; IF: 10.264 / 1.1404 / 2.3095).

5. Oleksandr Chernyavskiy, Lucie Kubínová: *Multi-photon excitation microscopy*, in *Proceedings of Advances in widefield and confocal fluorescence microscopy*, Ljubljana (Slovenia), March 13-14, 2008 (ISBN 978-80-7399-377-1).

Presented Publications

Libuše Váchová, <u>Oleksandr Chernyavskiy</u>, Dita Strachotová, Paolo Bianchini,

Zuzana Burdíková, Ivana Ferčíková, Lucie Kubínová, Zdena Palková

Architecture of developing multicellular yeast colony:
spatio-temporal expression of Ato1p ammonium exporter

(cover page)

IFs: 4.909 / 0.4909 / 0.4909

Libuše Váchová, Vratislav Šťovíček, Otakar Hlaváček, Oleksandr Chernyavskiy,

Luděk Štěpánek, Lucie Kubínová, Zdena Palková

Flo11p, drug efflux pumps, and the extracellular matrix
cooperate to form biofilm yeast colonies

(cover page)

IFs: 10.264 / 1.1404 / 1.6313

Oleksandr Chernyavskiy, Luca Vannucci, Paolo Bianchini,
Francesco Difato, Mustafa Saieh, Lucie Kubínová

***Imaging of mouse experimental melanoma in vivo and ex vivo
by combination of confocal and nonlinear microscopy***

(cover page)

IF: 1.85 / 0.4625 / 2.0938

Viviana Kozina, David Geist, Lucie Kubínová, Ernest Bilić, Hans Peter Karnthaler,
Thomas Waitz, Jiří Janáček, Oleksandr Chernyavskiy, Ivan Krhen, Davor Ježek

Visualization of Reinke's crystals in normal and cryptorchid testis

IFs: 2.588 / 0.2157 / 2.3095

Oleksandr Chernyavskiy, Lucie Kubínová

Multi-photon excitation microscopy